Design of Resource to Backbone Transmission for a High Wind Penetration Future

by

James Michael Slegers

A thesis submitted to the graduate faculty

in partial fulfillment of the requirements for the degree of

MASTER OF SCIENCE

Major: Electrical Engineering (Electrical Power Engineering)

Program of Study Committee:

James D. McCalley, Major Professor

Dionysios Aliprantis

Chris Harding

Iowa State University

Ames, Iowa

2013

DEDICATION

I would like to dedicate this thesis to my parents John and Sheryl and the rest of my family - who from a young age have encouraged my interests in math, science and engineering. I would like especially to thank my brother Joseph who understands me completely, no matter what the context. I would also like to thank my friends and colleagues for their guidance and support during my period of study in Ames.

TABLE OF CONTENTS

LIST OF TABLES

LIST OF FIGURES

ACKNOWLEDGEMENTS

I would like to take this opportunity to express my thanks to those who helped me with various aspects of conducting research and the writing of this thesis. First and foremost, Dr. James McCalley for his patience and guidance throughout this research and the writing of this thesis, as well as for providing me with means of financial support through the NSF and the EPRC. Second I would like to thank my committee members — Dr. Aliprantis whos classes shaped my understanding of wind energy and system dynamics, and Chris Harding. Last, I would like to thank all the students and industry engineer who gave me feedback in the course of this project.

ABSTRACT

In a high wind penetration future, transmission must be designed to integrate groups of new wind farms with a high capacity inter-regional "backbone" transmission system. A design process is described which begins by identifying feasible sites for future wind farms, identifies an optimal set of those wind farms for a specified future, and designs a reliable low-cost "resource to backbone" collector transmission network to connect each individual wind farm to the backbone transmission network. A model of the transmission and generation system in the state of Iowa is used to test these methods, and to make observations about the nature of these resource to backbone networks.

APPENDIX B. Transmission Line Loading: Considerations for the Use of High Temperature Conductors

B.1 Transmission Line Load Limitations

Transmission lines are physical structures, installed in the natural environment – an environment which subjects them to wind, rain, ice, snow, sunlight, and pollution. Beyond the natural environment, these structures exist in a human-developed environment. Structures must be designed to minimize damage to themselves, as well as preventing injury to humans and other structures. A successful design will be safe, reliable, and efficient. A few specific limitations will be described below, the consideration of which are required for a successful design.

Transmission lines will be designed to limit the distance that their conductors will sag, so that a minimum vertical clearance between the cables and the ground, the minimum distance to any local structure, and the minimum distance to other local transmission lines is maintained. This clearance must be guaranteed for a variety of conditions, including maximum high-temperature sag and maximum static load. Guidelines for establishing a maximum static load are outlined by the National Electrical Safety Council (NESC) in the US and the International Electrotechnical Commission (IEC) throughout the world, and generally define this load in terms of the amount of ice accumulation that is likely to occur on a given line. Another form of static loading is wind displacement, where a steady wind will act on a conductor. Ice accumulation and high winds both occur during the same part of the year, so lines must be rated to withstand both phenomena simultaneously. Cables have limited strength, so they must be designed to not exceed that strength even under heavy loading.

High temperatures cause conductors to expand and elongate. This effect causes the con-

ductors to sag. Thermal sag may be a limiting factor for the ampacity of a transmission line. Decreasing the sag of a cable can increase the capacity of the transmission line or decrease the number of support structures that a design requires. Sag can be decreased by several means — increasing the stringing tension of the cable, increasing the conductive material in a line (thus, decreasing its operating temperature), or using a high-temperature low-sag conductor which elongates less under increased temperatures.

Care must be taken to maintain the distances between individual conductors. Uncontrolled conductors which sway in strong winds may pass close to each other, causing arcing and short-circuit behavior. This is unacceptable. Many strategies are used to prevent this from occurring, including increasing the spacing between phases, adding mid-span spacers to limit conductor motion, or adjusting conductor tension.

Vortex shedding occurs when air becomes turbulent after passing cables. In some transmission line designs, this can cause Aeolian vibration, a constant hum of the cable. This vibration causes significant conductor motion, and can shorten the lifespan of the cable and the support structures due to fatigue. Aeolian vibration is only a significant concern for transmission lines built in a very specific scale of geometry, such that the frequency of vortex shedding behavior closely matches their natural frequency of vibration. It can be mitigated by adding conductor spacers, which change the natural frequency of the conductor. Vibration can also be mitigated by using unique conductors which dissipate mechanical energy or through conductors of unique geometries which spread the vortex-shedding behavior over a range of frequencies. In general, longer and heavier cables will be more resistant to vibration.

Ice shedding is a common event for lines which accumulate ice. When ice falls off of a conductor, it often comes off in large quantities. This sudden change in loading will cause the conductor to jump. This displacement is mostly vertical, rather than horizontal. This phenomena will be analyzed for lines that may accumulate ice, to show that in the event of ice-shedding, phase conductors will not be brought close enough to induce arcing. This is typically remedied by increasing the vertical spacing between conductors.

In some circumstances, terrain, weather, and wind in combination can produce galloping. Galloping is a violent motion of conductors which may cause displacements of cables by up to

10 feet in long spans. The displacement of galloping will typically be restricted to an elliptical zone around the static position of the line. Like Aeolian vibration, it may be reduced by adding phase-spacers. Slackening conductors may also reduce this behavior.

Generally, thicker (and thus heavier) conductors and longer spans will reduce the motion caused by wind or ice phenomena, at the cost of increased structural requirement at the suspension points and potentially greater sag.

B.2 Sag Calculation

The sag of a transmission cable is impacted by several phenomena including changes in heating, changes in loading, and long-term creep. The distance that a cable will sag depends on the length of the conductor span, the weight of the conductor, its initial tension, and its material properties. The cable itself will have a unit weight, core cross-section and diameter, conductor cross-section and diameter, and stress-strain curves for both the core and the conductor. It will also have a coefficient of thermal elongation.

In any overhead transmission line, there will be multiple support structures. The distance between any two structures is called a span. The cable in a single span of a transmission line can be described by a set of hyperbolic functions which describe catenary curves [86]. For a cable with a span-length l, weight w, and horizontal tension H, the maximum sag distance S (the vertical distance between the point of attachment and the cable, at the lowest point in the span) is described by the hyperbolic function:

$$S = \frac{H}{w}\left[\cosh\left(\frac{wl}{2H}\right) - 1\right] \tag{B.1}$$

Where

S — Maximum sag distance, in $ft.$

H — Horizontal tension at each end, in $lbs.$

w — Weight per unit length, in $lbs./ft.$

l — Span length, in $ft.$

and cosh is the hyperbolic cosine function. This function is nonlinear, and is not simple to work with for lines with multiple spans. For this reason, the function is often simplified by linearizing about $l = 0$.

$$S = S(0) + \frac{S'(0)}{1!}l + \frac{S''(0)}{2!}l^2 \dots$$

$$S'(l) = \frac{\partial S}{\partial l} = \frac{1}{2}\sinh\left(\frac{wl}{2H}\right)$$

$$S''(l) = \frac{w}{4H}\cosh\left(\frac{wl}{2H}\right)$$

$$S = 0 + \frac{1}{2}(0)l + \frac{\frac{w}{4H}(1)}{2!}l^2 + \dots$$

$$S \simeq \frac{wl^2}{8H} \tag{B.2}$$

The total length of the cable L in this span is described by the hyperbolic function:

$$L = \frac{2H}{2}\sinh\left(\frac{wl}{2H}\right) \tag{B.3}$$

This function is often linearized around l=0 as well:

$$L \simeq l + \frac{w^2l^3}{24H^2} \simeq l + \frac{8S^2}{3l} \tag{B.4}$$

$$\Delta L = L - l \simeq \frac{w^2l^3}{24H^2} \tag{B.5}$$

ΔL, the difference between L and l is referred to as the 'slack'.

A transmission line composed of multiple spans can be generalized using the principle of the *ruling span*[87]. In this generalization, a single span is formed which is representative of the entire transmission line. A span with these dimensions will have a sag which is equal to the sag that would be seen if the transmission line had equal spans, and the cable mounts could move freely. If the mounts are free to move, the horizontal tension from the cable at any point of attachment must be equal from both horizontal directions. For the ruling span itself, the tension at both ends is equal to the tension that would be found at each of the equal spans. This method is used in order to compare the behaviors of different conductor sizes and

materials, throughout a single transmission line. The ruling span S_R is the span length of this conductor. For a transmission line with n spans,

$$S_R = \sqrt{\frac{\sum S_i^3}{\sum S_i}} \tag{B.6}$$

In a real transmission line, conductors will be held in place by clamps attached to insulators, which may be stiff or free-hanging, but which will restrict the horizontal motion of the cable. Lines will also vary in elevation, which will change the distribution of weight of the conductors and thus affect the tension applied at the insulators.

Example

1-mile of a transmission line is to be re-conductored, using Drake 795-kcmil ACSR conductor. The line has a ruling span of 400-ft. Drake has a rated tensile strength (RTS) of 31,500 lbs. , and a per-unit weight of 1093 lb/1000ft. The line will have an initial horizontal tension of 18% RTS. Find the initial sag distance and the slack for the ruling span of this line.

$$l = 400ft.$$

$$H = 18\% \times 31500lbs. = 5670lbs.$$

$$w = \frac{1093lbs.}{1000ft.} = 1.093\frac{lbs.}{ft.}$$

First, find the sag, using the exact formula (B.1):

$$S = \frac{H}{w}\left[\cosh\left(\frac{wl}{2H}\right) - 1\right] = \frac{5670}{1.093}\left[\cosh\left(\frac{1.093 \times 400}{2 \times 5670}\right) - 1\right] = 3.856ft.$$

Next, apply the approximate formula(B.2):

$$S \simeq \frac{wl^2}{8H} = \frac{1.093 \times 400^2}{8 \times 5670} = 3.853$$

Now, calculate the slack, using the exact formula (B.3), and compare to the approximate formula (B.5):

$$\Delta L = \frac{2H}{w}\sinh\left(\frac{wl}{2H}\right) - l \qquad = 0.0991ft.$$

$$\Delta L \simeq \frac{w^2l^3}{24H^2} \qquad = 0.0991ft.$$

Example

For the line in the previous example, if the conductor was instead replaced with Tern 795-kcmil ACSR, which has a tensile strength of 22,100 lbs. and weight of 895 lbs./1000ft., find the new initial sag.

$$l = 400ft.$$

$$H = 18\% \times 22100lbs. = 3978lbs.$$

$$w = \frac{895lbs.}{1000ft.} = 0.895\frac{lbs.}{ft.}$$

$$S \simeq \frac{wl^2}{8H} = \frac{0.895 \times 400^2}{8 \times 3978} = 4.500ft.$$

Example

Find the ruling span for a transmission line with spans of {320-ft., 400-ft., 420-ft., 400-ft., 400-ft., 350-ft., 420-ft.}

$$S_R = \sqrt{\frac{320^3 + 400^3 + 420^3 \ldots}{320 + 400 + 420 \ldots}} = 391.7ft.$$

B.2.1 Thermal Elongation

Heat causes conductors to expand. As a conductor expands, it becomes longer and sags lower. The distance that a particular conductor expands is often described by a linear temperature coefficient α_T. The length of a simple conductor, for temperatures T near an initial temperature T_0 may be calculated as follows [87]:

$$L_T = (1 + a_T \times (T - T_0))\, L_{T_0} \tag{B.7}$$

Where

L_T — Length of the cable at temperature $T(^\circ\mathrm{C})$

L_{T_0} — Length of the cable at initial temperature $T_0(^\circ\mathrm{C})$

a_T — Coefficient of thermal expansion, $\frac{ft.}{ft.}\frac{10^{-6}}{^\circ\mathrm{C}}$

B.2.2 Stress-Strain Behavior

Conductor cables under tension will undergo deformation. Figure B.1 shows a stress-strain diagram for a simple conductor. Strain (elongation) of the conductor is mostly linear at low

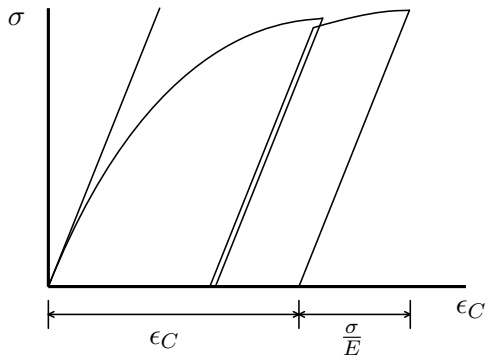

Figure B.1 Simple Stress-Strain Behavior

stress (tension). This linear behavior is considered elastic. As tension increases past the yield stress, some of the strain becomes permanent. After this point, if the cable is relaxed, it will shrink linearly, but will retain some deformation permanently. This permanent deformation is plastic deformation.

The length of a conductor in its range of elastic behavior, with respect to stress σ is represented by:

$$\begin{aligned} L_\sigma &= L \times (1 + \epsilon_\sigma + \epsilon_C) \\ \epsilon_\sigma &= \frac{\sigma}{E} = \frac{H}{EA} \end{aligned} \tag{B.8}$$

Where

L_σ — Length under stress σ, in $ft.$

L — Length under no stress, in $ft.$

ϵ_σ — Elastic strain, in $\frac{ft.}{ft.}$

σ — Stress, in $\frac{lbs.}{in^2.}$

E — Modulus of elasticity for the conductor, in $\frac{lbs.}{in^2.}$

A — Cross-sectional area of conductor, in in^2.

H — Tension applied to the conductor, in $lbs.$

ϵ_C — Plastic deformation of the cable, due to inelastic deformation and creep, in $\frac{ft.}{ft.}$

If a conductor is coated with a large enough amount of ice, it may be stretched past its yield stress. When the ice is eventually shed, the conductor will contract elastically, but will

still bear some permanent deformation.

Every transmission line cable is under some tension. Over time, this tension will tend to permanently stretch the cable. This behavior is known as creep. Creep has been modeled and parameterized for most types of cables. Transmission lines are long-term investments. They are typically used for 40 years or more, so it is important to design a line that will operate safely for many years in the future.

The elongation of a conductor under stress was described as simple and linear. In high-precision transmission design programs such as PLSS-CAD and SAGT, higher-dimension polynomials are used to express the load-strain curves, so that plastic deformations and creep can be calculated precisely.

B.2.3 Sag at High Temperatures

When a conductor undergoes thermal elongation, the length L of the cable increases while the span l remains the same. This results in a decrease in tension in the conductor. So, to find the sag distance of a hot conductor, we must consider both thermal expansion and strain under tension. The tension of a conductor and the temperature at which the cable was strung will be known or specified. To find the sag, you must find a tension H at which the length of the elongated cable is equal to the catenary cable's length [87]:

$$L = L_0(1 + a_T \times (T - T_0)) \left(1 + \frac{H - H_0}{EA} + \epsilon_C\right) \tag{B.9}$$

Where

L — Length at temperature T, in ft.

L_0— Initial length, in ft.

H — Horizontal tension at temperature T, in lbs.

H_0— Initial horizontal tension, in lbs.

T — Temperature, in °C

T_0— Initial temperature, in °C

Substitute in the linear approximation of cable length, from (B.4).

$$l + \frac{w^2 l^2}{24H^2} = \left(l + \frac{w^2 l^2}{24H_0^2}\right)(1 + a_T \times (T - T_0))\left(1 + \frac{H - H_0}{EA} + \epsilon_C\right) \tag{B.10}$$

Given temperature T, equation (B.10) can be solved for horizontal tension H. This tension H can in turn be used with (B.2) to calculate the sag.

Example

A 400-ft span of Hawk 477-kcmil ACSR conductor is originally tensioned at 20% RTS, on a 60 (15.5°C) day. The cable is rated at 75°C. Find the tension and sag of the cable at its original and rated temperatures. Assume no permanent elongation ($\epsilon_C = 0$). Hawk ACSR has the following properties:

$$A = 0.435 in.^2$$

$$_T = 19.3 \times \frac{10^{-6}}{°\mathrm{C}}$$

$$E = 11.5 MPsi$$

$$H_{RTS} = 19500 lbs.$$

$$w = 0.656 \frac{lbs.}{ft.}$$

$$T = 75°\mathrm{C}$$

$$T_0 = 15.5°\mathrm{C}$$

$$H_0 = 20\% \times 19500 lbs = 3900 lbs$$

Multiply (B.10) by H^2, rearrange as a polynomial, and solve for H:

$$0 = k_1 H^3 + k_2 H^2 + 0H - k_4$$

$$k_1 = \left(1 + \frac{w^2 l^2}{24H_0^2}\right)(1 + {}_T(T - T_0))\left(\frac{1}{EA}\right)$$

$$k_2 = \left(1 + \frac{w^2 l^2}{24H_0^2}\right)(1 + {}_T(T - T_0))\left(1 - \frac{H_0}{EA} + C\right) - 1$$

$$k_4 = \frac{w^2 l^2}{24}$$

Use MATLAB `roots()` command:

```
roots([k1 k2 0   k 4 ])
ans =
  −2277.2 + 1701.1i
  −2277.2 − 1701.1i
   1774.0
```

Only the positive-real root has physical meaning here. $H = 1774lbs$. Now, compute the sag:

$$S \simeq \frac{wl^2}{8H} = 7.40ft.$$

Example

After 10 years, the transmission line in the previous example has undergone creep, and now has a permanent elongation of 0.04% ($\epsilon_C = 0.0004$). Find the new tension and creep at 75°C. Recompute k_2, and solve for the tension.

```
roots([k1 k2 0   k 4 ])
ans =
   −3776.3
   −2514.5
    1509.4
```

Again, only the positive-real root has physical meaning here. $H = 1509.4lbs$. Now, compute the sag:

$$S \simeq \frac{wl^2}{8H} = 8.692ft.$$

B.2.4 Sag with Ice Loading

Ice accumulation will significantly increase the weight of a transmission line cable, contributing to increased sag. A cable must be shown to maintain adequate ground clearance, even under heavy ice loading. The NESC standards for clearance provide guidelines for calculating the final sag of a transmission line, based on the region in which the line is to be installed. Transmission owners may impose their own stricter standards, based on the weather conditions to which the line is likely to be exposed. The following methodology is based on the NESC standard [88], and is diagrammed in Figure B.2.

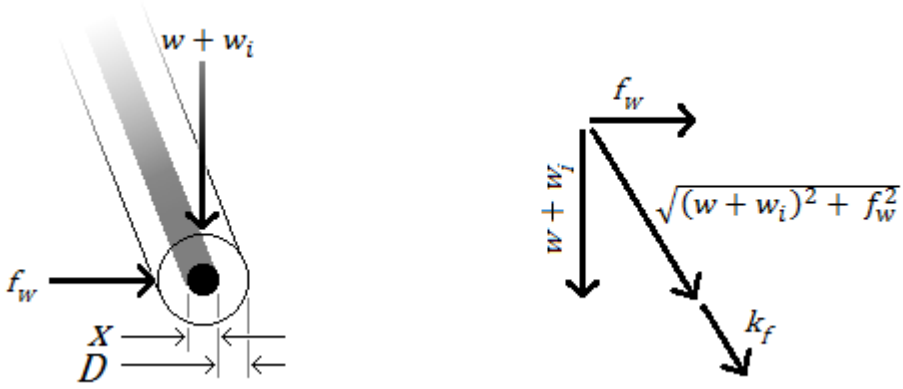

Figure B.2 NESC Ice-Loading Methodology

The sag of the cable must be calculated for a force F which is the resultant of the weight of the ice-coated cable, the horizontal force from wind, and an adder k_f. F is defined:

$$F = \sqrt{(w + w_i)^2 + f_w^2} + k_f \tag{B.11}$$

Where

F — The magnitude of the resultant force acting on every foot of the cable, in lbs/ft

w — Weight of the conductor itself, in lbs/ft

w_i— Weight of the accumulated ice, in lbs/ft

f_w— Force from winds acting perpendicular to the conductor, in lbs/ft

k_f— A constant additional force, added to the resultant, in lbs/ft

The weight of the conductor itself should be available from vendor documentation. Ice loading is usually described in terms of 'x inches of ice' — that is, a cylindrical layer of ice x inches thick, coating the conductor. The volume of x inches of ice is given:

$$v_i = \left[\left(\frac{D}{24} + \frac{x}{12}\right)^2 - \frac{D^2}{4}\right]\pi \tag{B.12}$$

Where

v_i — Volume of ice per unit length, in ft^3/ft

D — Diameter of the conductor, in in

x — Thickness of ice coating the conductor, in in

NESC Loading Criteria	Zone 1 (Heavy)	Zone 2 (Medium)	Zone 3 (Light)
Radial ice (in)	0.5	0.25	0
Horizontal wind pressure (lbs/ft^2)	4	4	9
Temperature T (°C)	-20	-10	-1
Constant k_f (lb/ft)	0.3	0.2	0.05

Figure B.3 NESC Criteria for Ice-loaded Sag Calculations

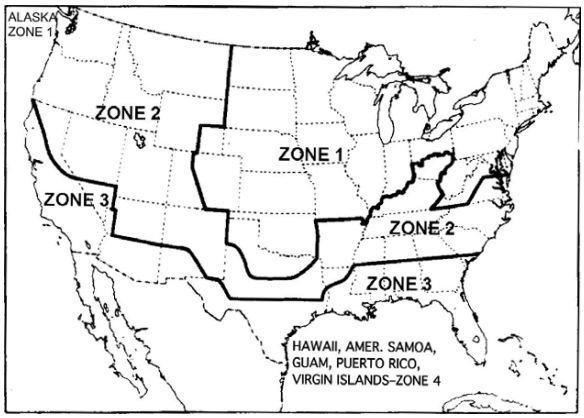

Figure B.4 NESC Loading Zones

The weight w_i of the conductor with x inches of radial ice is $w_i = v_i \times \rho_i + w$, where ρ_i is the density of ice ($57lb/ft^3$) and w is a the weight of the conductor itself in lbs/ft.

Force f_w is calculated based on a constant pressure P_w applied to the exposed cross-sectional area of the ice-coated cable. f_w can be calculated from $f_w = P_w \times \left(\frac{D}{12} + \frac{2x}{12}\right)$. Table B.2.4 lists the standard parameters required for NESC loading tests, by loading class. Figure B.4 shows the regions where those loading classes will be generally applicable [88].

The elongation of an ice-loaded conductor is calculated similarly to calculation of thermally-induced elongation, but here the weight the cable is substituted with the force from ice-loading, so that the slack on the left hand of the equation is representative of the length of a catenary curve with the ice-load, and the right hand represents the elongation of the cable which was originally tensioned at H_0 at temperature T_0. Ice loaded sag S can be found by solving B.13 for tension H, then computing S from (B.2).

$$l + \frac{\boldsymbol{F}^2 l^3}{24H^2} = \left(l + \frac{w^2 l^3}{24H_0^2}\right)(1 + a_T \times (T - T_0))\left(1 + \frac{H - H_0}{EA} + \epsilon_C\right) \tag{B.13}$$

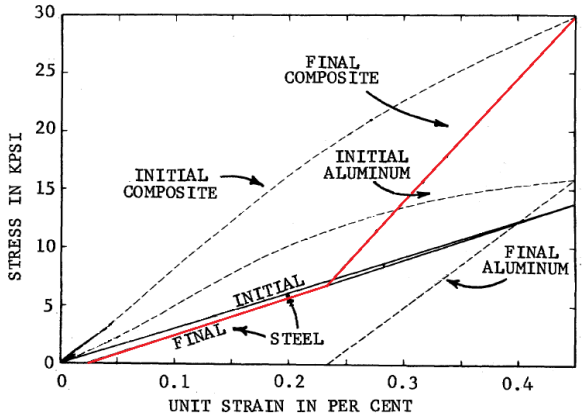

Figure B.5 Composite Stress-Strain behavior of 24/7 636kcmil ACSR

B.2.5 Behavior of Layered Cables

Most conductors used in new transmission lines are composed of two or more materials. The most common — Aluminum Conductor, Steel Reinforced (ACSR) — has a stranded steel core surrounded by layers of strain-hardened aluminum. The steel core provides a great deal of strength, while the aluminum has very good conductive properties. The two materials utilized in this cable will expand at different rates due to temperature and tension. At low temperatures, ACSR can be approximated as a combination of the properties of both steel and aluminum. At higher temperatures, most of the tension will be imparted on the steel core, and it will elongate much like a regular steel cable. High temperatures impart slack to the cable, so cables operating at heightened temperatures will be under decreased tension.

To account for this combination, we must look at the stress-strain behavior of both materials, and show how they combine. Figure B.5 shows the load-strain curves of aluminum and steel superimposed over each other [89]. Initial curves are the inelastic behavior of the layer under stress. Final curves represent the elastic behavior, after inelastic strain has occurred. The red curve is the composite elastic behavior of the conductor.

The aluminum conductor layer and steel core have differing cross-sectional areas and different elastic moduli, as well as different thermal expansion coefficients. The creep behavior of each material is different as well. If the aluminum conductor layer exhibits more creep behavior over time, the relationship between these curves may also shift. Core materials, which are typ-

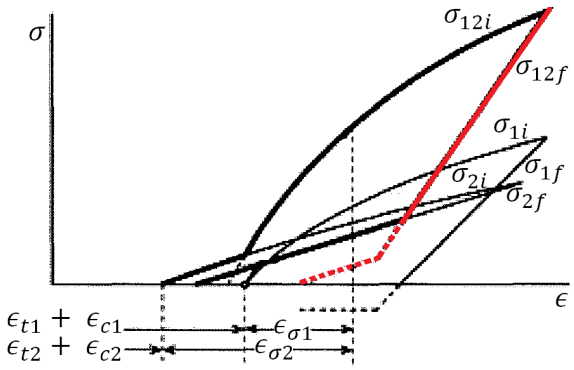

Figure B.6 Composite Stress-Strain behavior with Creep and Thermal Elongation

ically stronger than the conductor material, often exhibit very little creep. Figure B.6 shows the effect of creep and thermal elongation on the composite load-strain behavior [90]. Curve 1 describes the aluminum, curve 2 describes the core, and curve 12 describes the composite behavior. Notice that the values of $\epsilon_{t1} + \epsilon_{c1}$ and $\epsilon_{t2} + \epsilon_{c2}$, which represent thermal elongation and creep, are unequal. The dotted line indicates the behavior of the aluminum strands under compression, which may also be modeled. Under high compression, a cable may begin to 'birdcage', wherein its component strands separate and unwind near the compression clamps that hold the cable.

As shown in Figures B.5 & B.6, there is often a transition point above which the behavior of the cable is dependent on both the core and conductive layer, and below which the conductive layer is in compression and the behavior is dependent solely on the core material. When a strung cable is heated, its thermal elongation causes excess sag and lower tension. The transition point to core-only behavior will be seen at a fixed temperature, which depends on the original stringing tension of the cable and its layers. High-temperature cables are often designed to shift the location of that transition point to a lower temperature, so that the whole load is applied to the core, which often has a lower coefficient of thermal elongation.

B.3 Ampacity of a Conductor

Ampacity is the current-carrying capacity of a cable. A cable will have a maximum operating temperature, which may be limited by the physical makeup of the cable, or may be

limited by a maximum amount of allowable sag. High current in a cable will cause significant resistive heating. At the same time, direct sunlight will also heat the cable. The cable will be cooled by wind, through convective heat transfer. All of these factors impact the temperature of the cable, so to establish a thermal current-carrying limit, some operating conditions must be assumed.

B.3.1 Heat Balance Equation

The thermal behavior of a conductor can be calculated using a heat-balance equation. The simple steady-state model of a cable is described as follows [91] [92]:

$$Q_C + Q_R = Q_S + Q_{EM} \tag{B.14}$$

Where

Q_R — Radiant heat loss per unit length, in W/ft

Q_C — Convective heat loss per unit length, in W/ft

Q_S — Heating from solar insolation per unit length, in W/ft

Q_{EM}– Heating due to AC resistance per unit length, in W/ft

B.3.2 Q_R — Radiant Heat Loss

Radiant heat loss is thermal energy emitted by electromagnetic waves, due to the temperature difference between an object and its environment. Radiant heat loss can be estimated based on the geometry of a conductor, its temperature, and the ambient temperature of the environment around it, demonstrated in B.15.

$$Q_R = k_s k_e \left(\frac{D\pi}{12}\right)(T^4 - T_a^4) = 0.138 \times 10^{-8} k_e D(T^4 - T_a^4) \tag{B.15}$$

Where

k_s — Stefan-Boltzmann constant, for black-box radiation $= 0.5268 \times 10^{-8} \frac{W}{ft^2 K^4}$

k_e — Emissivity, typically between 0.23 and 0.91 – low for new cables,
high for dirty or oxidized cables, usually around 0.5 (unitless)

D — Diameter of the cable, in in (So that $\left(\frac{D\pi}{12}\right)$ represents the surface area of the cable in $\frac{ft^2}{ft}$)

T — Cable temperature, in K

T_a — Ambient temperature, in K

B.3.3 Q_C — Convective Heat Loss

Convective heat loss is the effect of heat transfer due to fluid (in this case, air) passing in contact with an object (here, a metal conductor). Convective heat loss for conductor cables has been studied, and fitted to several different relationships. Forced convection is the heat loss due to wind forcing air past a cable. If there is no wind, natural convection occurs. To compute convective loss, you must first compute the Nusselt number Nu, which itself will be based on the Reynolds number Re. Re describes the turbulence of the air flowing past the conductor. In the IEEE Standard 738 [91], forced convection heat loss Q_C is approximated, based on the work of House and Tuttle[93]:

$$Re = \frac{v\rho\frac{D}{12}}{\eta/3600} \tag{B.16}$$

$$\begin{aligned} \mathrm{Nu_{lo}} &= 0.32 + 0.43Re^{0.52} \text{ for laminar (smooth) air flow } (Re < 1000) \\ \mathrm{Nu_{hi}} &= 0.24Re^{0.6} \text{ for turbulent air flow } (Re \geq 1000) \end{aligned} \tag{B.17}$$

$$k_\phi = 1.194 - \cos(\phi) + 0.194\cos(2\phi) + 0.368\sin(2\phi) \tag{B.18}$$

$$Q_{C,force} = \pi\lambda k_\phi \ \mathrm{Nu}(T - T_a) \tag{B.19}$$

Where

v — Component of wind speed which is normal to the cable, in $\frac{ft}{s}$

D— Diameter of the cable, in in

ρ — Specific mass of air, in $\frac{lb}{ft^3}$

η — Dynamic viscosity of air, in $\frac{lbs}{ft-hr}$

λ — Thermal conductivity of air, in $\frac{W}{ft°\mathrm{C}}$

Temperature T_{film} (°C)	Dynamic viscosity η $(lb/ft\text{-}hr)$	Air density ρ (lb/ft^3) Sea level	5,000 ft	10,000 ft	15,000 ft	Thermal conductivity of air (λ) $(\frac{W}{ft°C})$
0	0.0415	0.0807	0.0671	0.0554	0.0455	0.00739
10	0.0427	0.0779	0.0648	0.0535	0.0439	0.00762
20	0.0439	0.0752	0.0626	0.0517	0.0424	0.00784
30	0.0450	0.0728	0.0606	0.0500	0.0411	0.00807
40	0.0461	0.0704	0.0586	0.0484	0.0397	0.00830
50	0.0473	0.0683	0.0568	0.0469	0.0385	0.00852
60	0.0484	0.0661	0.0550	0.0454	0.0373	0.00875
70	0.0494	0.0643	0.0535	0.0442	0.0363	0.00898
80	0.0505	0.0627	0.0522	0.0431	0.0354	0.00921
90	0.0515	0.0608	0.0506	0.0418	0.0343	0.00943
100	0.0526	0.0591	0.0492	0.0406	0.0333	0.00966

Figure B.7 Material Constants of Air

ϕ — Angle between wind direction and the cable

T, T_a — Cable temperature and ambient temperature, in °C

For natural convection, heat loss is approximated by [91]:

$$Q_{C,nat} = 0.283\rho^{0.5}D^{0.75}(T - T_a)^{1.25} \tag{B.20}$$

Forced convection and natural convection occur at the same time, so Q_C is the vector sum of $Q_{C,forced}$ and $Q_{C,nat}$. For the IEEE Standard, however, it is suggested that convective cooling should be chosen to be the largest of $Q_{C,forced}$ or $Q_{C,nat}$ [91]. This is a conservative assumption, so that convective cooling is not overestimated.

Values of ρ, η, and λ are widely available, usually in fluid dynamics texts. A brief table of these values is given in Table B.7 [91]. T_{film} represents the average temperature between the cable and the environment, $T_{film} = (T - T_a)/2$. Other models for calculating Q_C exist which may take other atmospheric conditions into consideration, and which utilize different approximations.

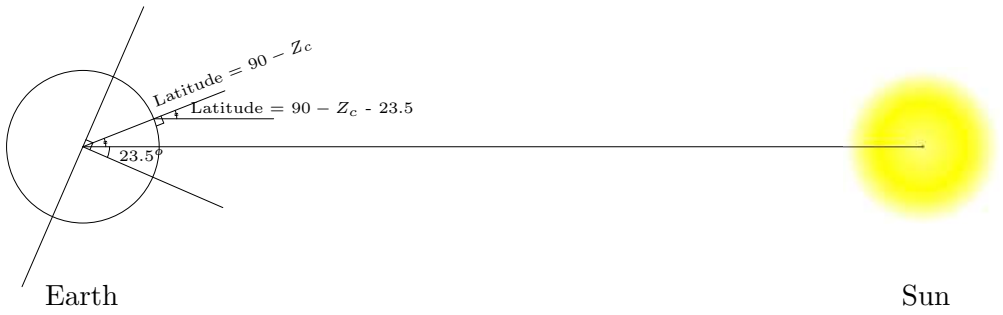

Figure B.8 Solar Elevation Angle

B.3.4 Q_S — Heat Gain from Solar Radiation

Heat from solar radiation is absorbed by the projected area of the cable. The amount of heat varies by the location of the line, its direction with respect to the sun, the reflectiveness of its surface, and the clarity of the air. The IEEE Standard model for calculating Q_S is given:

$$Q_S = k_a Q_{se} \frac{D}{12} \sin(\omega) \tag{B.21}$$

$$\omega = \arccos\left[\cos(H_C)\cos(Z_c - Z_l)\right] \tag{B.22}$$

Where

k_a — Solar absorption coefficient, unitless. In most practical situations, this value is around 0.5 [92]

Q_{se}— Elevation-adjusted solar and sky heat flux rate, in $\frac{W}{ft^2}$. Values will range from 79-125 $\frac{W}{ft^2}$, with a practical value of 1000 $\frac{W}{m^2} = 93\frac{W}{ft^2}$ indicating a typical sunny day[92].

ω — Effective angle of incidence of the Sun's rays

H_C— Altitude of the Sun, in *deg* above the horizon. At its peak, this angle will be equal to $H_C = 90° - (Latitude - 23.5°)$, as illustrated in Figure B.8 [92]

Z_c — Azimuth of the Sun, in *deg* clockwise from due North (in the Northern Hemisphere, this will be 180° at noon)

Z_l — Azimuth of the transmission line, in *deg* clockwise from due North (an East-West line will have an azimuth of 90 or 270 *deg*)

In many practical cases, sufficient accuracy may be acheived with the simpler approximation [94]:

$$Q_S = k_a Q_{se} \frac{D}{12} \tag{B.23}$$

B.3.5 Q_{EM} — AC Losses

AC current losses represent the resistive loss of a conductor due to AC current. This calculation uses the AC resistance of the cable, which represents not only the resistivity of the cable itself, but also the skin effect caused by alternating current. DC resistance increases nearly linearly with temperature. AC resistance follows this increase closely. The change of AC resistance with temperature can be approximated by a linearization around a reference temperature. Resistance and resistive losses are calculated:

$$R_{T,AC} = R_{20,AC} \times (1 + \alpha_R(T - 20)) \tag{B.24}$$

$$Q_{EM} = I_{RMS}^2 R_{T,AC} \tag{B.25}$$

Where

I_{RMS} — RMS current flowing in a single conductor

$R_{20,AC}$— AC resistance of the conductor, at 20°C, in Ω/m

$R_{T,AC}$— AC resistance of the conductor, at temperature T, in Ω/m

α_R — Temperature coeffiient of resistance, in $^\circ\text{C}^{-1}$

Values for $R_{20,AC}$ and α_R can be found on spec-sheets for conductors.

B.3.6 I_{RATED} — Ampacity of a Conductor

GIven Q_R,Q_C, Q_S, and Q_{EM}, for some operating temperature T, the ampacity of a cable can be calculated. Equation (B.14) is used, and (B.25) is substituted in, resulting in:

$$Q_C + Q_R - Q_S = I_{RMS}^2 R_{T,AC} \tag{B.26}$$

Which can be reorganized as:

$$I_{RMS} = \sqrt{\frac{Q_C + Q_R - Q_S}{R_{T,AC}}} \tag{B.27}$$

Equation (B.27) will specify the rated steady-state current of a conductor for the environmental conditions used in the calculation of Q_C, Q_R, and Q_S. The conditions assumed for these calculations have typically been conservative assumptions about the windspeed and temperature during periods when the cable will run near its limit — for instance, a wind speed of 2 ft/s and an ambient temperature of 40°C. Limits may be specified for several distinct parts of the year — for instance, a cable may have separate ratings for summer and winter months.

A great deal of research has been done on the topic of Flexible AC Transmission Systems (FACTS). In many of these systems, the sag and temperature of one or all of the conductor spans in a transmission line will be monitored continuously, as will local weather conditions. Ampacity may be recalculated in real-time, based on present conditions. If these conditions are more favorable than the conservative conditions mentioned above (for instance, the temperature is below peak summer temperature, or there is significant wind), then the conductor may be allowed to operate at a higher ampacity during that time period. These systems could lead to better utilization of new or existing transmission lines.

Example

A new 161-kV transmission line is built at an altitude of 1000-ft, using Drake 795-kcmil ACSR conductors, one conductor per phase. The conductor temperature is limited to 75 °C in normal operation. Find the thermally-limited power rating of the line, when the ambient temperature is 40 °C, and wind is blowing at 2 ft/s. Drake ACSR has the following properties:

$$A = 0.7264 in^2$$

$$D = 1.108 in$$

$$R_{75,AC} = 0.139\frac{\Omega}{mi} = 0.139\frac{\Omega}{mi}\frac{1mi}{5280ft} = 2.6326 \times 10^{-5}\frac{\Omega}{ft}$$

$$v = 2 ft/s$$

$$T_\alpha = 75°\text{C} = 348K$$

$$T = 40°\text{C} = 313K$$

Assume:

$$Q_{SE} = 93\frac{W}{ft^2}$$

$$k_a = 0.5$$

$$k_e = 0.5$$

$$\eta = 0.0499\frac{lb}{ft-hr}(\text{Interpolated from Figure B.7})$$

$$\rho = 0.0614\frac{lb}{ft^3}(\text{Interpolated from Figure B.7})$$

$$\lambda = 0.00909\frac{W}{ft°\text{C}}(\text{Interpolated from Figure B.7})$$

Radiant Heat Loss:

$$Q_R = k_s k_e D\pi(T^4 - T_a^4) = (0.5268 \times 10^{-8}\frac{W}{ft^2K^4})(0.5)(\frac{1.108in}{12})\pi(348^4K^4 - 313^4K^4)$$

$$Q_R = 3.8724\frac{W}{ft}$$

Convective Heat Loss:

$$Re = \frac{v\rho D/12}{\eta/3600} = \frac{(2ft/s)(0.0614lb/ft^3)(1.108/12ft)}{(0.0499/3600\frac{lb}{ft-s})}$$

$$Re = 818.0 \text{ (Re } < \text{ 10,000, Low turbulence)}$$

$$Nu = 0.32 + 0.43Re^{0.52} = 0.32 + 0.43(818)^{0.52} = 14.384$$

$$Q_C = \pi\lambda Nu(T - T_a) = \pi\left(0.00909\frac{W}{ft-K}\right)(14.38)(348K - 313K)$$

$$Q_C = 14.373\frac{W}{ft}$$

Solar Heating:

$$Q_S = k_a D Q_{SH} = (0.5)(\frac{1.108}{12}ft)(93\frac{W}{ft^2})$$

$$Q_S = 4.2935\frac{W}{ft}$$

Rated Conductor Current:

$$I_{RMS} = \sqrt{\frac{Q_C + Q_R - Q_S}{R_{75,AC}}} = \sqrt{\frac{(14.373 + 3.8724 - 4.2935)W/ft}{26.326\mu\Omega/ft}} = 727.99A$$

Thermal MVA Rating:

$$P_{RATED} = \sqrt{3}V_{ll}I_{RMS} = \sqrt{3}(161 \times 10^3V)(727.99A)$$

$$P_{RATED} = 203.01MVA$$

B.4 High Temperature, Low Sag Transmission Technologies

Constructing new transmission lines is often difficult politically, and can be expensive. Transmission planners would like to maximize the carrying capacity of new and existing lines, to reduce the number of new lines that must be built.

Operating transmission lines at high current rates causes significant conductor heating. Heating of conductors can cause significant conductor sag, which will either limit the length of spans or require taller support structures. Conventional conductors may also be limited by their own maximum operating temperature, above which they will physically degrade.

One way to increase line capacity is to replace the conductors (reconductor) with larger or stronger conductors. The scope of this upgrade will be limited by the size of the cables that the original support structures can hold, and the sag of the new cable. Engineers may also seek to reconductor a line due to mechanical problems such as vibration or galloping.

There are a variety of types of cable which have been developed which may perform better than conventional conductors. These cables are significantly more expensive, so they are not often used for new transmission lines, but they may present economical options for upgrading existing lines.

B.4.1 Conventional Conductors (AAC, AAAC, ACSR)

Most of the transmission lines in service today utilize aluminum (AAC), aluminum-alloy (AAAC) or steel-reinforced aluminum conductors (ACSR). Aluminum is utilized because of its high conductivity and low weight density. Steel is added in ACSR for extra strength, and for its resistance to sag.

The aluminum used in conventional conductors carries all or most of the tension in the cable. In order to provide adequate strength, the aluminum strands are work hardened (or cold worked) to increase their physical strength. This increase in strength is due to dislocations in the crystal structure of the material which make it difficult for layers of atoms to slip past each other. These dislocations also slightly increase the electrical resistance of the conductor.

Heating a cold-worked conductor can cause it to anneal. When a material anneals, the dis-

locations in its crystal structure begin to release, reducing the materials strength. Conductors should not be operated at temperatures which cause them to anneal. This is the basis of the operating temperature of most conductors.

Aluminum (AAC) cables are made entirely from extruded aluminum strands. They are simple and cheap. But, they are only as strong as the aluminum they are composed of, and they exhibit significant sag due to aluminum's low elastic modulus. Some cables are made with an aluminum alloy (AAAC), which gives them higher tensile strength. Aluminum cables are not commonly used for new transmission projects, but many are still in use on older transmission lines.

Steel reinforced aluminum conductor (ACSR) cables are made with a steel cable at their core, surrounded by strands of aluminum. Both the steel and aluminum are cold-worked, so each provides some portion of the tensile strength of the cable. When heated, elongation is most closely related to the steel core, which stretches less than the aluminum.

AAC, AAAC, and ACSR cables are limited to operating temperatures of 90-100°C. Above that limit, the aluminum conductor will begin to anneal and lose strength. Often, transmission lines with these cables have been designed to operate below 60-75°C, to limit their sag.

B.4.2 Aluminum Conductor, Steel Supported (ACSS)

Another kind of cable, steel supported aluminum conductors (ACSS), known in the older literature as SSAC, and euphemized with the term "Sad SAC" is a sag-resistant steel-cored conductor [89]. Unlike ACSR, ACSS is almost entirely supported by its steel core. The aluminum strands are not cold-worked in manufacture, so they have the same properties as fully annealed aluminum. The steel core provides most of their tensile strength.

The behavior of ACSS is a composite of the steel core and annealed aluminum, though the aluminum carries little of the load, because of its low yield strength. The operating temperature of ACSS is not limited by the properties of aluminum, since the aluminum is already fully annealed. Instead, the temperature limitation comes from the properties of the steel core, which has an annealing temperature around 240°C (though, the surface temperature may be significantly cooler). This is significantly higher than ACSR or AAAC. A higher temperature

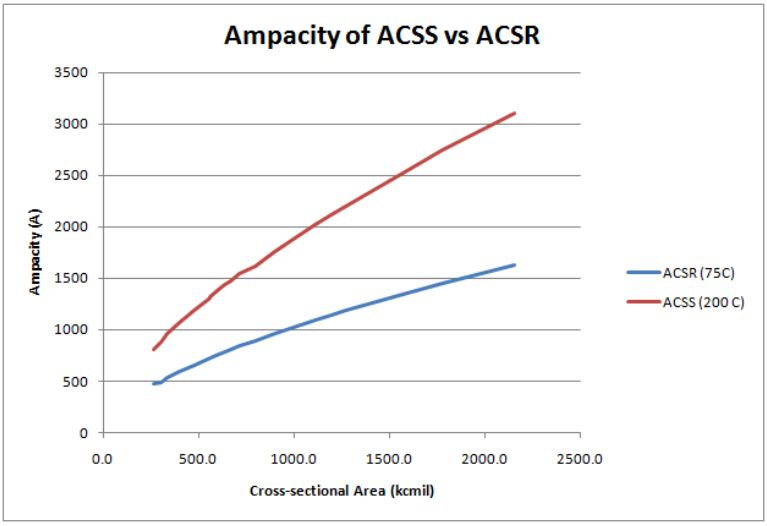

Figure B.9 Ampacity of ACSR and ACSS cables

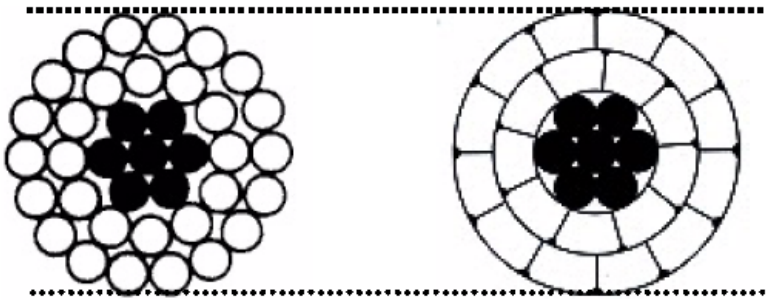

Figure B.10 Cross-sectional Comparison of Roundwire and Trapwire

limit means that a greater amount of current can be passed without weakening the cable. Figure B.9 shows the rated ampacity of equivalent ACSR and ACSS cables at rated operational temperatures (75 °C and 200 °C, respectively), ambient temperature of 25 °C and wind at 2 ft/s [95].

ACSS and some other high temperature conductors are often built as compact conductors. These conductors are composed of trapezoidal wires which have a closer fit than round wires of the same cross-sectional area (see Figure B.10) [96]. Compact ('Trap Wire') conductors can replace conventional conductors of the same diameter, while increasing the cross-sectional area of the conductor. This will lower the resistance per-mile, and increase the ampacity of the

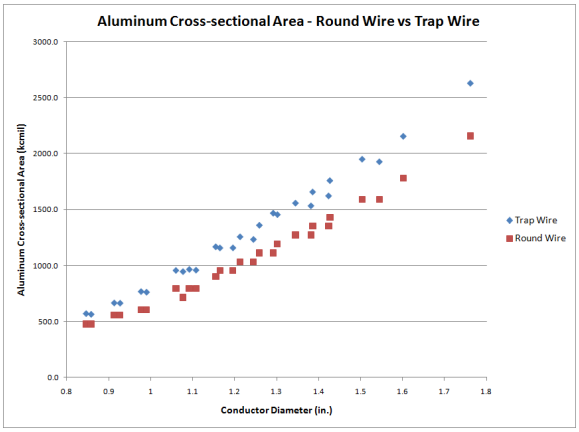

Figure B.11 Cross-sectional Area Comparison of Roundwire and Trapwire

cable. Figure B.13 compares the amount of aluminum in ACSS conductors with round strands vs. those with trap wire. Resistance is inversely proportional to cross-sectional area. Figure B.10 shows the ampacity of common sizes of ACSR, ACSS, and ACSS/TW cables of the same diameter [97][95].

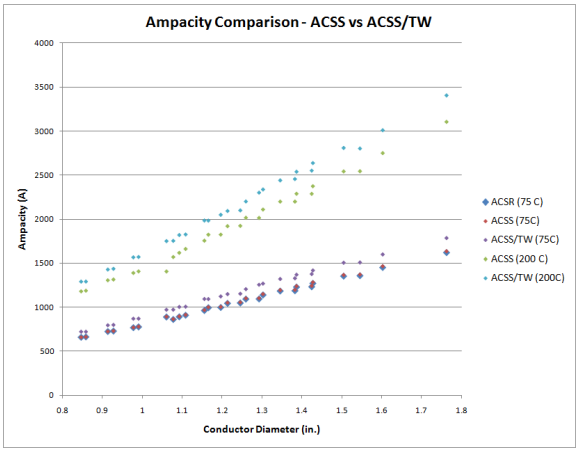

Figure B.12 Ampacity Comparison of Roundwire and Trapwire

The high-temperature sag behavior of ACSS is generally better than that of ACSR. Often, the steel core will be pre-tensioned prior to installation, to prevent creep behavior. Plastic elongation of the annealed aluminum layer does not contribute significantly to final sag, since the slack is picked up by the elastic behavior of the steel core.

ACSS is among the cheapest high-temperature conductor technologies, with a bulk price 1.5-2x that of ACSR. It is composed of the same materials that make up ACSR, and is a commonly used to replace ACSR when uprating transmission lines.

B.4.3 (Super) Thermal-Resistant Aluminum Alloys — (Z)TACSR and (Z)TACIR

Aluminum alloy conductor strands have been developed that are resistant to annealing far above the normal temperatures of pure aluminum. These conductors are strain hardened and are alloyed with small amounts of other metals, such as Zr. The alloyed metals change the nature of the metallic crystal, increasing its annealing temperature. Alloys differ, depending on the desired operating temperature of the conductor. These alloys are often listed as Thermal-resistant and Super-thermal-resistant aluminum alloys (TAl and ZTAl). These alloys are designed to operate continuously at 150 °C and 200 °C respectively [98].

(Super) Thermal-resistant Aluminum Alloy Cables, Steel Reinforced ((Z)TACSR) are formed similarly to ACSR, but utilize TAl or ZTAl rather than the typical work-hardened aluminum conductor stranding. TAl and ZTAl materials are also used in GTASCR and ACCR cables, as mentioned below.

TAl and ZTAl have slightly lower conductivities than are seen in regular aluminum, so larger cables may be required in order to achieve the ampacity of equivalent ACSR cables.

B.4.4 Composite Cores — ACCC and ACCR

Composite-cored cables have cores formed from fibers embedded in a matrix material. These materials tend to be very strong, and have small coefficients of thermal expansion. When the aluminum conductor layer elongates, it quickly imparts the whole load of the cable onto the core, which exhibits very little elongation with respect to heat. In high-temperature settings, these cables exhibit much less sag than ACSR or ACSS.

Aluminum Conductor, Composite Core (ACCC) , licensed by CTC Cable Corporation, utilizes a composite core made of stranded carbon-fiber and epoxy, and fully annealed aluminum as a conductor. The composite core is very strong, and has an extraordinarily small coefficient of thermal elongation . The operating temperature of ACCC is limited by its composite core, since

the aluminum conductor is already fully annealed. Although the manufacturers rate the core at 180°C, independent testing has shown that above 150°C, the core will begin to permanently deform. Above 170°C, the core will begin to degrade, permanently losing strength [96]. This thermal operating range is lower than that of ACSS cables of a similar size. But, within its thermal operating range, the high-temperature sag characteristics of ACCC are much better than ACSS.

Figure B.13 Composite-core Cables. Left: ACCC. Right: ACCR [96]

3M sells a cable technology called Aluminum Conductor, Composite Reinforced (ACCR) which has a composite core made of Aluminum-Oxide strands embedded in aluminum, and conductor strands composed of a hardened heat-resistant Al-Zr alloy. The behavior of the core is similar to that of steel, but is significantly lighter, and is itself conductive. The alloy used in ACCR allows it to operate at 210°C normally, and 240°C in emergency [99]. The thermal expansion of ACCR is larger than that of ACCC, but still quite a bit less than that of ACSR or ACSS. Cross-sections of ACCC and ACCR are shown in Figure B.4.4

3M markets their product exclusively for uprating transmission lines through reconductoring. Their literature suggests that ACCR has costs 3-6 times those of comparably sized cables, but is cost-effective in situations where 30-40% of existing support structures would have to be replaced in order to uprate with ACSR.

Like ACSS, ACCC and ACCR cables are often sold as trap-wires. Due to the complexity

of their composite cores, these cables are more expensive than ACSR or ACSS cables.

B.4.5 Invar Core - TACIR

Invar is the trade-name of 64FeNi, an alloy that has a low coefficient of thermal expansion at high temperatures. It can be used in place of a steel core to improve the sag behavior of a conductor. Invar and composite cores are usually paired with high-temperature aluminum conductor strands, in order to minimize the sag that is caused by operating at high temperature [100].

Thermal Resistant Aluminum Alloy Conductor, Invar Reinforced (TACIR) is one type of cable which utilizes an Invar core. TACIR and ZTACIR (the Super-Thermal-resistant variety) utilize aluminum alloy conductor strands that can be operated at high temperatures without degrading their strength.

Invar steel has a coefficient of thermal elongation between those of composite cores and galvanized steel. It has been used extensively for new transmission lines in Japan and Korea, where right of way is extremely limited.

B.4.6 Gap-Type Conductors — Gap-Type (Super) Thermal-Resistant Aluminum Alloy Conductor, Steel Reinforced (G(Z)TACSR)

In a gap-type conductor, a stranded core is surrounded by a hollow cylinder of trap-wire, forming a gap between the core and the conductor which is filled with thermal-resistant grease (see Figure B.14) [101]. When it is strung, special techniques will be used to impart the entire load on the core. In this way, the transition point between core-behavior and combined behavior can be controlled.

G(Z)TACSR utilizes a thermal-resistant aluminum alloy conductor, much like ACCR. The core is generally made of galvanized steel, the same as would be found in ACSS or ACSR. The gapped nature of this conductor makes it complicated to install. It may require specialized hardware, in order to pre-tension the core.

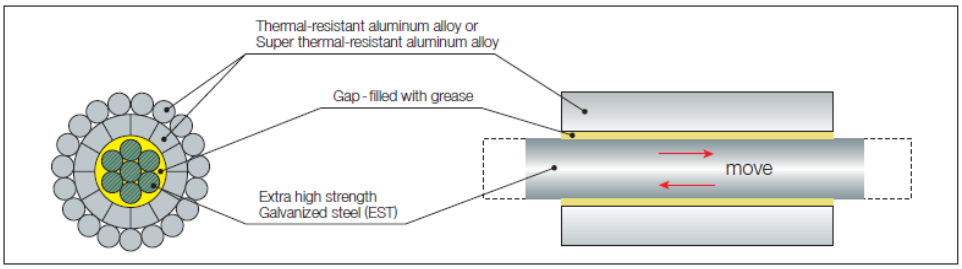

Figure B.14 Gap-type Conductor Construction [101]

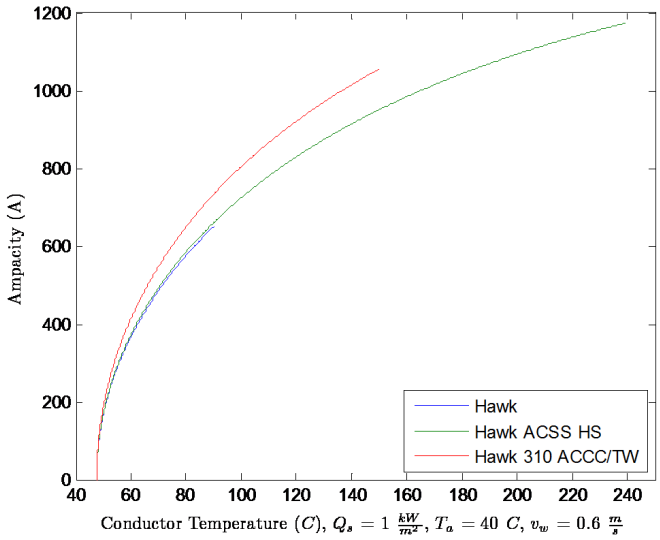

Figure B.15 Comparison of Thermal Ampacity Limits for 3 Varieties of Conductor

B.5 Comparison of High-Temperature Conductors

High temperature conductors are often used to uprate existing transmission lines, utilizing their decreased thermal expansion, higher allowable temperatures, or their higher cross-sectional area to increase ampacity without increasing final sag.

Increases in allowable operating temperature correspond to significant increases in ampacity. Figure B.15 demonstrates the relationship between temperature and ampacity for 3 conductors of the same diameter. The 'Hawk' ACSR cable has the lowest operational temperature limit. The 'Hawk ACSS' cable has slightly less resistance, since it is made with annealed aluminum

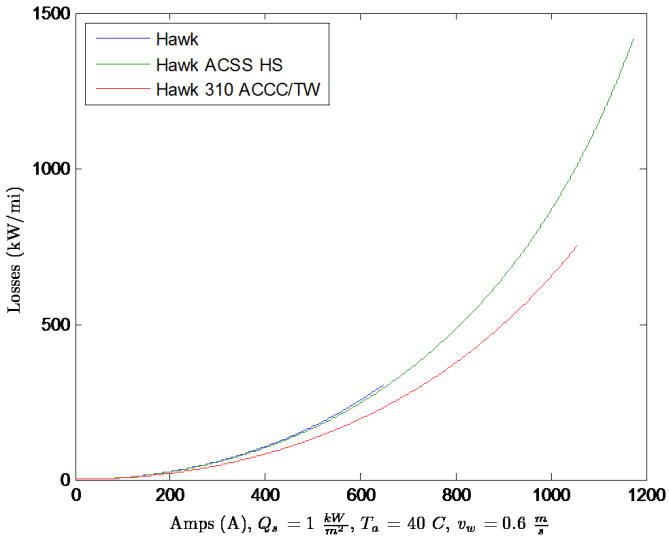

Figure B.16 Real Power Loss (kW/mile) for 3 Varieties of Conductor

which is slightly more conductive than worked aluminum. This allows it to operate at a slightly higher current than the ACSR. The ACCC/TW conductor is a trap-wire, and the core takes up very little space. As a result, its conductive 0-worked aluminum has quite a bit more cross-sectional area and less resistance than the ACSS cable, which causes it to heat up less than the ACSS. This comparison was done for environmental conditions identified below the figure.

Operating at higher current will incur greater $I^2R(T)$ losses. R increases with temperature and current, so losses will increase at slightly greater than the square of current. This relationship is visualized in Figure B.16 for the same 3 conductors as before. It should be clear that the significant increases in ampacity allowed by the high-temperature conductors come at the cost of significantly higher joule loss.

Losses decrease nearly linearly with resistance. Resistance in conductors is proportional to cross-sectional area of a conductor. Ampacity also increases with added cross-sectional area. Thus, one way to improve ampacity and decrease losses is to use cables of the same type with larger cross-sectional areas. This has been the primary strategy when uprating lines, prior to the emergence of high-temperature alternatives.

The primary feature of all the cable technologies above is their improved sag behavior.

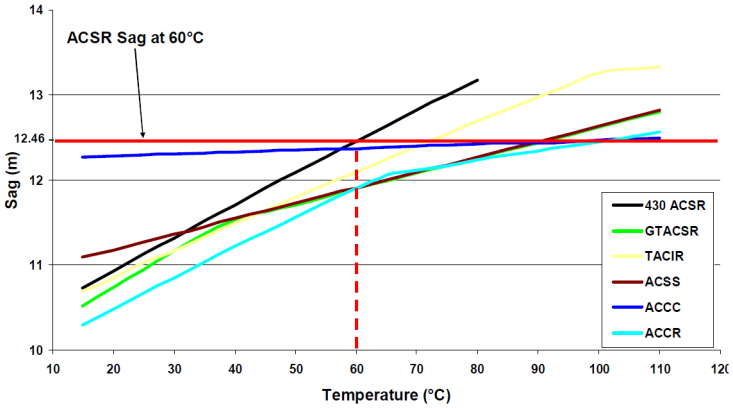

Figure B.17 Sag vs. Temperature for Each Conductor Type

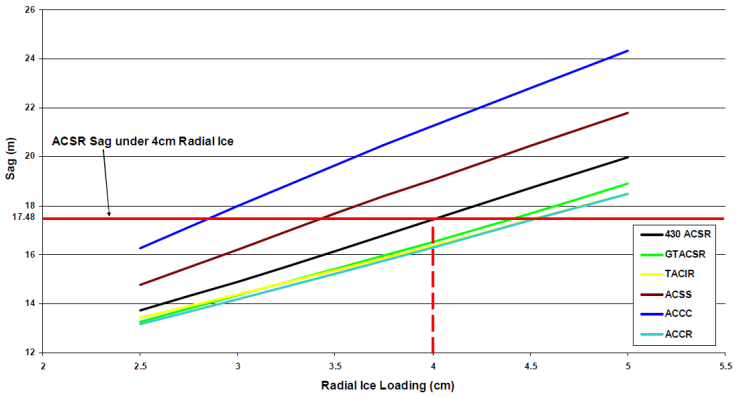

Figure B.18 Sag vs. Radial Ice Loading for Each Conductor Type

Figure B.17 & Figure B.18 show the results of a study by an Irish utility [100], which compared the theoretical performance of a variety of high-temperature conductors in order to find which would be most appropriate for re-conductoring an existing 220kV transmission line.

All 5 of the high-temperature conductors outperform the ACSR alternative under high-temperature conditions. It is clear where some of the cables transition all of their load to their cores. For ACCR, the transition point is around 65 °C. For GTACSR, it is even lower, since most of the tension should already be applied to the core at its initial stringing temperature, which is around 20 °C. Other conductor technologies such as ACSR and TACIR have very high transition temperatures, which will not be reached under normal operating conditions.

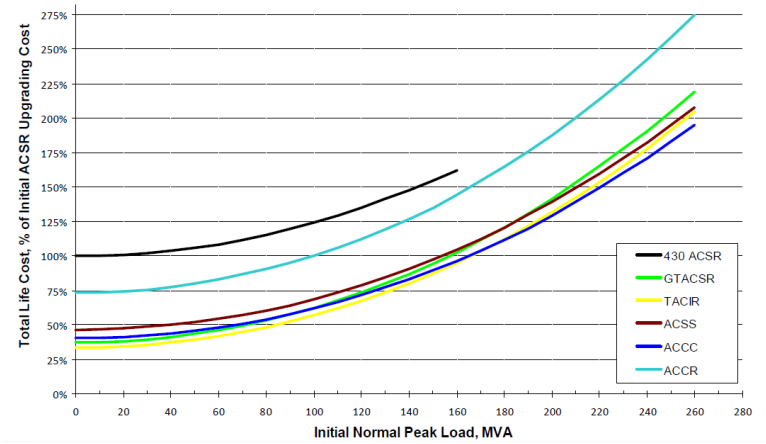

Figure B.19 Cost of Uprating, based on Normal Peak Loading

Figure B.18, however, shows that some conductors may be inappropriate for regions with heavy ice-loading. The performance of ACCC and ACSS is significantly worse than that of ACSR. These two conductors have fully annealed aluminum conductor strands, which require their cores to carry the entire tension load. The core of ACCC has a particularly low elastic modulus, and small cross-sectional area. As a result, even though this cable has low sag under high current, it experiences significant ice-loaded sag.

High-temperature conductors have higher material costs than standard conductors, ranging from 1.3-6x the cost of equivalent ACSR cables. They also operate at high temperatures, incurring significant losses, and requiring specialized high-temperature hardware. However, their improved sag capabilities allow these cables to be used in longer spans, or at lower sags, reducing the number of towers that would have to be built or replaced.

Figure B.19 comes from the same report as above, and shows the relative present-value cost of uprating a 220kV transmission line. Construction costs were added to losses (capitalized over 25 years), for a range of peak loading values. Curves for individual conductor technologies are terminated where that cable would meet its physical limitations. They were compared against a scenario in which the existing transmission line was reconductored with ACSR cable, to be capable of providing 150MVA of capacity. The cost at 0 MVA represents construction costs alone, since losses will be zero.

It is evident that the construction cost of uprating with any of the high-temperature technologies will be significantly lower than uprating with ACSR. Uprating with ACSR would likely require many of the support structures to be raised or replaced, in order to meet existing sag requirements at a higher temperature. The high-temperature conductors would not require as many structural upgrades, evidently.

The cost difference between ACSR and the other conductors varies. ACSS, which is physically very similar to ACSR, has a cost of 1.5-2x that of ACSR. According to 3M, the cost of ACCR is 3-6x that of ACSR. The rest of the cable technologies appear to lie within that range of 1.5-6x.

APPENDIX C. Compact and HSIL Transmission Line Design Considerations

C.1 Introduction

It is advantageous to both transmission line developers and to landowners to minimize the space required for a transmission line. This is the basic idea behind compact transmission line design. Compact transmission lines are not fundamentally different from traditional transmission lines, but because they are designed to take up less space, they require some considerations that may not be necessary when designing transmission lines with more traditional form factors [102].

Traditional transmission lines were designed very conservatively — with wide spaces between phase conductors which made the risk of phase-to-phase flashovers very low, and left surface voltage gradients at very low levels. They had simple wooden frame designs which were cheap and easy to build.

In recent years, building new transmission lines has been difficult. Often, the largest impediment to a transmission project is securing right-of-way access. Landowners are hesitant to comply with developers who they may see as outsiders, without their interests in mind. Some people balk at the spectre of a transmission line cutting across their property, altering the perceived beauty of the landscape. Neighbors may fear that their property values will decrease. These concerns [103] are very common.

This resistance has a cost to developers, who must go through a great deal of work to procure the easements necessary for new transmission lines. As a result, transmission developers have found ways to decrease the right of way necessary for new projects. This is often done by reusing existing right of way, occupied by existing distribution lines. Developers often choose

to uprate existing transmission lines to higher voltages or to conductors with higher current ratings.

Compact line design is the result of this space-saving strategy. New transmission lines are designed to take up far less lateral space by utilizing modern materials and altering tower geometries. The structures in these modern designs are simpler and require less space, reducing their visual impact. These designs reduce phase-to-phase and phase-to-structure distances, which in turn increase voltage gradients on conductors and reduced flashover voltage thresholds. Methods first used in EHV transmission design are utilized in order to guarantee that audible noise (AN), radio noise (RN), and EM fields are kept at acceptable levels. Reduced phase spacing has the added benefit of increasing the surge impedance loading of lines, which can increase the loading limit of long lines.

The horizontal cross-section of compact lines is decreased using several methods. Triangular and vertical arrangements of phases are used, rather than horizontal arrangements, in order to decrease the width of the structure. Steel pole structures and composite insulators are often used as well. These materials have increased strength, and can be used to support the lines with less material.

Figure C.1a shows a traditional support structure, as well as several typical compact structures. Traditional 'H-frame' structures were built of wood, and often utilized suspended ceramic insulators. Compact lines are typically built with tubular steel poles or single wooden poles, and suspended on composite insulators. As in Figures C.1b and C.1c, post-insulators are often used which provide structural support, requiring fewer steel pole arms. Some designs use v-shaped configurations of insulators to accomplish a similar function. Vertical structures with steel or wooden poles tend to be taller than H-frame structures, but take up less lateral space.

An emphasis is placed on controlling the motion of conductors, so that they can be spaced closer together without risking flashovers. Post insulators, and insulators in bracing positions are used to reduce motion at the point of suspension. Span lengths can be decreased, in order to decrease the physical motion of conductors. Phase-to-phase spacers may also be utilized to guarantee adequate spacing.

Insulators must be designed to adequately protect from flashovers. Phase-to-phase spacing

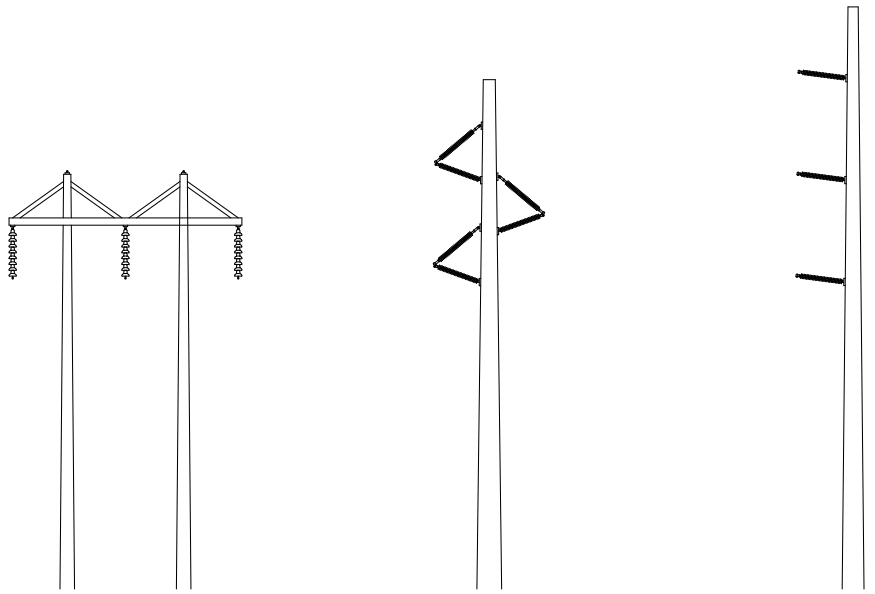

Figure C.1 (a) Horizontal 'H'-frame, (b) Vertical delta design with bracing post- and line-insulators, (c) Vertical design with post insulators

must be designed to limit voltage gradients and EM fields. Bundling can be used at lower-than-traditional voltages in order to further limit surface gradients. Shield wires and well-calibrated surge arrestors are used to further insulate the decreased air gaps against lightening-induced voltage surges.

As long as proper design considerations are followed, compact lines should operate no less reliably than traditional lines, and should not cause high numbers of complaints due to audible or radio noise. Design studies suggest that the cost of construction of these lines is not significantly higher than traditional designs [104]. But, the decreased cross-section may make such lines seem more agreeable to neighbors and lease holders.

Decreasing phase-to-phase spacing often has the added effect of increasing the Surge Impedence Loading (SIL) of a line. Surge Impedence Loading is the transfer level at which the reactive losses of the line match the capacitive reactance of the line, resulting in a transfer of all real power. Lines with high SIL can handle larger transfers of real power without violating voltage or stability limits, so lines with close phase-spacing will be better for long-distance transmission of AC power. Short transmission lines tend to be limited more by thermal effects

than by voltage or stability effects.

C.2 Phase Spacing and Conductor Motion

One of the primary insulators for overhead transmission lines is air. Transmission lines are mechanically designed to maintain adequate air gaps under a variety of environmental conditions, in order to prevent phase-to-phase and phase-to-tower faults. Wind and ice phenomena can significantly impact the behavior of conductors in the natural enviroment, so great care is taken to prevent these phenomena from reducing phase-to-phase spacing and causing faults.

Methods for calculating sag due to static ice and wind loading were covered in Appendix B. Conductor loading due to ice should be considered for a variety of credible scenarios, in order to assure that phase-to-phase faults do not occur. In traditional horizontal phase arrangements, unequal ice loads are unlikely to cause phase-to-phase faults. Compact designs, however, frequently feature conductors aligned in the same vertical plane. Unequal loading of conductors, inaccurate tensioning, or excessive vibration may cause a conductor to stray into proximity of a conductor above it. On top of this, phase-to-phase spacing is reduced in these designs. For this reason, a study of conductor motion is very important in compact lines.

C.2.1 Clearances

Sufficient clearance must be guaranteed such that under most normal conditions, phase-to-phase clearance, phase-to-tower clearance, and phase-to-obstacle clearance is maintained. These clearances must be maintained with respect to several voltages and voltage surges.

Clearances are more precisely described as voltage withstand distances. The ability of a dielectric (for transmission line clearances, this is air) to withstand a voltage is described as a probability distribution. For a given distance, a 50% withstand voltage will be defined, and a standard deviation will be either defined or assumed. Assuming that withstand voltages have a nearly normal distribution, an air gap of distance L has a 98% withstand voltage $V_{98\%}$ of $V_{98\%} = V_{50\%} - 2.05\sigma$, where σ represents the standard deviation of the withstand voltage of the air dielectric.

Minimum phase-to-ground clearances are specified by the National Electric Safety Code (NESC) for a number of environments [88]. These clearances are designed to account for peak operating voltages, switching-surge levels (transient peak voltages caused by switch openings and closings), elevation, and distance to obstacles, among other factors. Phase-to-tower clearances are maintained by utilizing adequate insulation. Post insulators and line insulator in bracing configurations are often used in compact transmission lines, so phase-to-structure clearances are fixed, and phase-to-tower clearances often do not depend on conductor motion.

Voltage surges due to switching are described as p.u. proportions of peak system voltage. In general, an EHV line must be designed to withstand switching surges of 1.75 - 2.5 p.u. Transient models of the network are used to simulate switching events, and a voltage crest level is selected to represent a switching surge overvoltage that will be exceeded very rarely — typically, only 2% of switching events. The switching-surge withstand strength of air has been measured empirically, and can described by (C.1)[105]:

$$V_{50\%,ss} = K_{g,ss} K_a 1080 \ln(0.46L + 1) \tag{C.1}$$

Where

$V_{50\%}$ — Peak switching surge voltage which an L meter air gap will withstand 50% of the time, in kV

L — Air gap distance, in m

$K_{g,ss}$ — Gap factor describing air gap geometry

K_a — Correction factor for altitude

$K_{g,ss}$ is a correction factor to relate the strength of a rod-plane gap to that of the geometry being studied. A list of appropriate gap factors is given in Table C.1 [92]. K_a is a correction factor due to the decreasing dielectric strength of air at high altitudes — presented as Table C.2. The required withstand voltage of an air gap between a conductor and another object (the tower, another conductor, the ground) will be given at a confidence level. For transient events, this level is frequently given as 90% (that is, air will withstand a voltage surge of peak magnitude $V_{90\%}$ in 90% of instances). If the 90% withstand voltage is greater than or equal to the 2% switching surge peak voltage, the probability that a given switching surge will

Gap Type	Switching Surge $K_{g,ss}$	Lightening Surge $K_{g,ff}$	Power-Frequency Voltage $K_{g,pf}$
Rod-to-plane	1.00	1.00	1.00
Conductor-to-obstacle	1.30	1.08	1.16
Conductor-to-plane	1.15	1.04	1.09
Conductor-to-tower	1.45	1.12	1.22
Conductor-to-conductor	1.60	1.16	1.26

Table C.1 Gap Factors K_g

Altitude	Altitude factor K_a			
(m)	up to to 200 kV	from 201 kV to 400 kV	from 401 kV to 700 kV	from 701 kV to 1100 kV
0	1.000	1.000	1.000	1.000
500	0.970	0.975	0.982	0.987
1000	0.938	0.946	0.959	0.970
2000	0.870	0.883	0.906	0.923
3000	0.798	0.815	0.844	0.867

Table C.2 Altitude Factor K_a

exceed the breakdown voltage of air will be far less than 1%. The dielectric strength of air due to switching surges can be assumed to have a standard deviation of $\sigma_v = 5 - 6\%$. A 90% probability level can be calculated:

$$V_{90\%} = (1 - 1.29\sigma_v)V_{50\%} \tag{C.2}$$

Voltage surges due to lightening are much faster than switching surges, and the resistance of air dielectric to these rapid surges is slightly different than that of slow surges. Lightening surges may be greater than 3x times the peak system voltage. The withstand voltage for lightening will again be selected to represent a level which will rarely be exceeded. Lightening has been well-studied, and there are many ways of measuring the risk probabilities of lightening strikes. A lightening surge insulation level will be based on these statistical methods, and will represent an acceptable level of risk, usually expressed as outages per 100 miles of line per year. Several aspects of tower design may be manipulated to decrease lightening flashover risk, such as proper arrangement of shield wires and use of surge arresters. Lightening withstand voltage can be calculated:

$$V_{50\%,ff} = K_{g,ff}K_a 530L \tag{C.3}$$

Phase-to-phase clearance has been a topic of some study. All power lines must be designed to withstand lightening-induced surges and switching surges, under static conditions (no motion). Many kinds of conductor motion can reduce phase-to-phase clearance, so it is important to consider conductor motion in the design of a transmission line. These are largely mechanical issues, caused by wind and ice cover. When considering conductors in motion, phase-to-phase clearances are based on power-frequency voltages, rather than on switching surge or lightening surge voltages. It is assumed that the probability of both a transient surge occuring and two conductors in motion coming into close proximity of each other at the same time is very low. All air gaps must adequately withstand the largest power-frequency voltages that are expected on the line. If a long line is open on one end and uncompensated, the capacitive charging of the line may cause a significant power-frequency overvoltage. Withstand voltages must account for

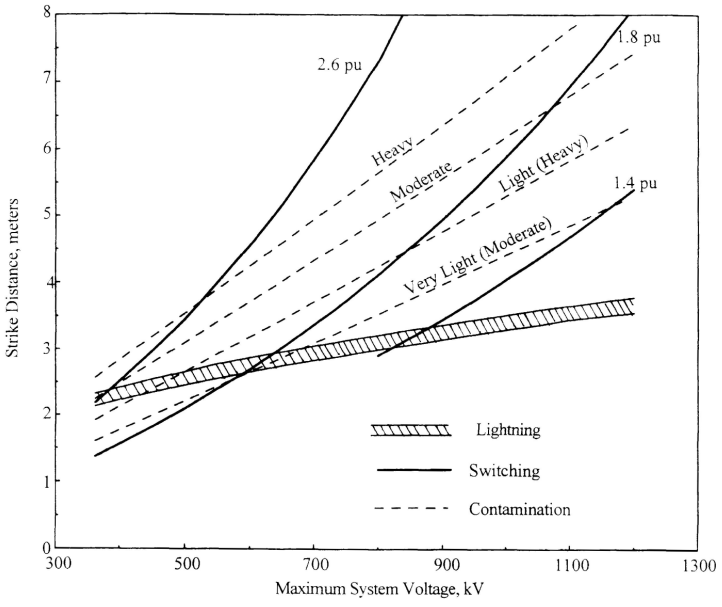

Figure C.2 $V_{50\%}$ Voltage withstand requirements for Power Frequency Voltage, Switching Surges, and Lightening Surges

the possibility of these voltage levels. Figure C.2 compares voltage withstand requirements for a variety of voltage considerations.

Power-frequency flashover withstand voltages can be calculated from the emperically derived curve in (C.4)[106].

$$V_{r.m.s.50\%} = K_{g,pf} K_a 750 \ln(1 + 0.55L^{1.2}) \tag{C.4}$$

Since, unlike transient switching and lightening events, power-frequency voltage occurs over long periods of time, power-frequency withstand voltages must be set at a higher withstand probability. Dielectric resistance to power-frequency voltage is assumed to have a standard deviation around $\sigma_v = 3\%$, but withstand voltage is required to be $3\sigma_v$, corresponding to a 99.9%probability.

There is some evidence that for high-magnitude surges, the peak phase-to-phase voltages may be significantly less than $\sqrt{3}\times$ phase-to-ground surge voltages [107]. An approximate relationship between phase-to-phase and phase-to-ground switching overvoltages is shown in C.3. For lightening surges, Kiesling suggests $V_{pp,ff} = 1.2V_{pg,ff}$ [92]. For power-frequency

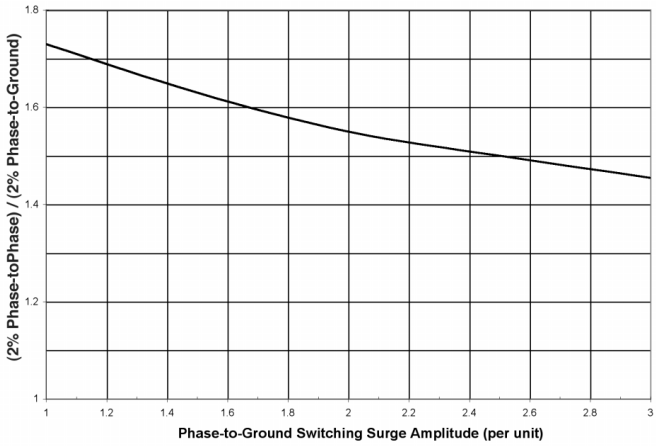

Figure C.3 p.u. Voltage withstand requirements $V_{50\%,pp}/V_{2\%,pg}$

voltages, $V_{pp,pf} = \sqrt{3}V_{pg,pf}$.

Withstand distances can be calculated from desired withstand voltages by inverting the withstand voltage equations.

For switching surges:

$$L_{90\%,ss} = 2.17 \exp\left[\frac{V_{ss}}{1080 K_a K_{g,ss}(1 - 1.29\sigma_v)} - 1\right] \tag{C.5}$$

For lightening-unduced surges:

$$L_{90\%,ff} = \frac{V_{ff}}{530 K_a K_{g,ff}(1 - 1.29\sigma_v)} \tag{C.6}$$

For power-frequency voltage:

$$L_{99.9\%,pf} = 1.64\left[\exp\frac{V_{pf,rms}}{750 K_a K_{g,pf}(1 - 3\sigma_v)} - 1\right]^{0.833} \tag{C.7}$$

Withstand distances only represent the insulating properties of air gaps. When designing insulation, insulator strands will be selected which have adequate withstand voltages, even when wet or dirty.

Figure C.4 shows the results of a survey done by EPRI, using data from real compact transmission lines — some of which were uprated from lower voltage transmission lines. The Phase Spacing Ratio is the ratio of the actual phase-to-phase spacing distance L_{pp} over the spacing required to insulate against a peak power frequency voltage $L_{pp,pf}$. While, overall, it

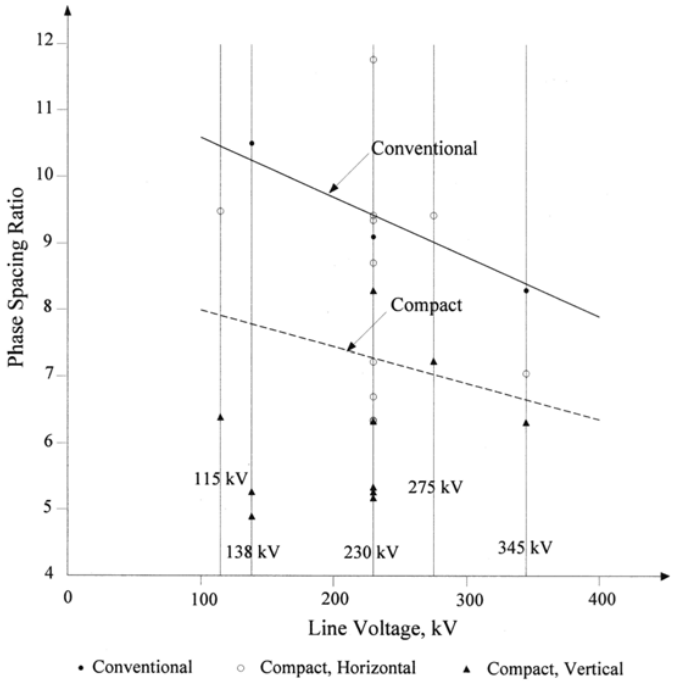

Figure C.4 L_{pp} / $L_{pp,pf,98\%}$, for Traditional and Compact Transmission Lines

shows that compact transmission line phase spacing in compact line is decreased, the value of that decrease varies significantly between individual lines.

Example:

A 161kV transmission line is to be built. Its maximum expected operating voltage is 1.05 p.u. It is to be built in Iowa, where the altitude is 300m above sea level. It must be built to withstand 90% switching surges of peak magnitude 2.5 p.u. and 90% of lightening surges of peak magnitude 3.0 p.u. Find the a) phase-to-tower and b) phase-to-phase wishstand distances for 1) switching surges, 2) lightening surges, and 3) power-frequency withstand.

1a) The tower is grounded, so phase-to-tower distance is based on phase-to-ground voltage. Phase-to-ground withstand voltage for switching surges:

$$V_{pg,ss} = \frac{161kV}{\sqrt{3}} \cdot \sqrt{2} \cdot 1.05 \cdot 2.5 = 345kV$$

From C.2 and C.1,

$$K_a = 0.982$$

$$K_{g,ss} = 1.45$$

For phase-to-tower switching surges, the required withstand distance is

$$L_{90\%,pg,ss} = 2.17 \exp \frac{V_{pg,ss}}{1080 K_a K_{g,ss}(1 - 1.29\sigma_v)} = 2.17 \exp \frac{345}{1080 \cdot 0.982 \cdot 1.45(1 - 1.29 \cdot 0.06)} = 1.036m$$

2a) Phase-to-tower withstand voltage for lightening surges:

$$V_{pg,ff} = \frac{161kV}{\sqrt{3}} \cdot \sqrt{2} \cdot 1.05 \cdot 3.0 = 414kV$$

The lightening surge flashover withstand voltage for this gap is:

$$K_{g,ff} = 1.12$$

$$L_{90\%,pg,ff} = \frac{V_{pg,ff}}{530 K_a K_{g,ff}(1 - 1.29\sigma_v)} = \frac{414}{530 \cdot 0.982 \cdot 1.12(1 - 1.29 \cdot 0.03)} = 0.739m$$

3a) The power-frequency phase-tower withstand voltage is approximately:

$$V_{pf,pp-rms} = 1.05 \cdot 161kV/sqrt3 = 97.9kV$$

$$L_{99.9\%,pg,pf} = 1.64 \left[\exp \frac{V_{pf,pg-rms}}{750 K_a K_{g,pf}(1 - 3\sigma_v)} - 1 \right]^{0.833} = 1.64 \left[\exp \frac{97.9}{750 \cdot 0.982 \cdot 1.22 \cdot (1 - 3 \cdot 0.03)} - 1 \right]^{0.833} = 0.294m$$

1b) Now, find the phase-to-phase withstand distances. Estimate $V_{pp,ss}$ from $V_{pg,ss}$, using Figure C.3 to find the likely peak phase-to-phase overvoltage.

$$V_{pp,ss} = 1.49 \cdot V_{pg,ss} = 514kV$$

$K_{g,ss} = 1.60$ **for a conductor-to-conductor gap. Therefore:**

$$L_{pp,ss} = 2.17 \exp \frac{V_{pg,ss}}{1080 K_a K_{g,ss}(1 - 1.29\sigma_v)} = 2.17 \exp \frac{514}{1080 \cdot 0.982 \cdot 1.60(1 - 1.29 \cdot 0.06)} = 1.102m$$

2b) Similarly, phase-to-phase lightening surge flashover withstand distance is calculated:

$$V_{pp,ff} = 1.2 \cdot V_{pg,ff} = 497kV$$

$$L_{90\%,pp,ff} = \frac{V_{pp,ff}}{530 K_a K_{g,ff}(1 - 1.29\sigma_v)} = \frac{497}{530 \cdot 0.982 \cdot 1.16(1 - 1.29 \cdot 0.03)} = 0.856m$$

3b) Finally, power-frequency phase-to-phase withstand distance is calculated

$$V_{pf,pp-rms} = 1.05 \cdot 161kV = 169.5kV$$

$$L_{99.9\%,pg,pf} = 1.64 \left[\exp \frac{V_{pf,pp-rms}}{750\sqrt{3} K_a K_{g,pf}(1 - 3\sigma_v)} - 1 \right]^{0.833} = 1.64 \left[\exp \frac{293.6}{750 \cdot 0.982 \cdot 1.26 \cdot (1 - 3 \cdot 0.03)} - 1 \right]^{0.833} = 0.468$$

C.2.2 Types of Conductor Motion

Wind and ice loading can cause a variety of types of conductor motion around which or against which a line will be designed.

C.2.2.1 Blowout

Blowout is the most basic conductor motion. Blowout refers to the magnitude of the horizontal displacement of a conductor, due to wind. This is most commonly caused by steady winds. Gusts of wind can cause more dynamic blowout, though the behavior will be significantly damped by the weight of the conductor itself.

Wind will exert pressure on a conductor, orthogonal to the conductor itself. For high-speed winds, that pressure can be estimated to be equal to [88]:

$$P = \frac{\rho}{2} V^2 \tag{C.8}$$

Where

P — Pressure, in Pa

ρ — Air density, in kg/m^3. Typically, around 1.225 kg/m^3

V — 5-minute average wind speed at conductor height, in m/s

Wind speeds should be selected to represent the highest wind speed expected over a period of time. From the pressure calculated in C.8, the force exerted on the conductor per unit length can be calculated:

$$F_w = P \frac{d}{100} C_f, \tag{C.9}$$

where d is the diameter of the conductor in cm, C_f is a force coefficient (assumed to be 1.0 for conductors), and F_w is force per unit length, in N/m. Blowout should be calculated for the maximum sustained wind speed. This is the method used in the NESC estimation of force due to wind. There are more accurate methods for calculating force due to wind —- the method shown above is a conservative estimate. Work published by CIGRÈ has suggested that this method consistently leads to overestimations of force, and suggests the linear approximation

given in C.10 [104]. Trapezoidal (compact) conductors and self-damping conductors have been shown to have lower drag coefficients than traditional stranded conductors, and the effctive force on these conductors will likely be less than traditional stranded conductors.

$$F_{N/m} = 0.0265 \cdot d_{cm} V_{m/s}, \text{ or}$$

$$F_{lb_f/ft} = 0.00675 \cdot d_{in} V_{mi/h} \tag{C.10}$$

Where

$F_{N/m}, F_{lb_f/ft}$ — Force per length of conductor, in N/m and lb_f/ft respectively

d_{cm}, d_{in} — Diameter of conductor, in cm and in respectively

$V_{m/s}, V_{mi/h}$ — Wind speed, in m/s and mi/h respectively

To calculate blowout, a transmission line is modeled as a point mass on a pendulum. Specify the weight per length of the conductor and force per length on the conductor. Then, set the moment of the pendulum to zero, and solve for the angle θ as shown in Figure C.5. Blowout angle θ and blowout distance d_{bo} are calculated from:

$$F_w \cos\theta = F_m \sin\theta$$

$$\frac{F_w}{F_m} = \frac{\sin\theta}{\cos\theta}$$

$$\theta = \arctan\frac{F_w}{F_m} = \arctan\frac{F_w}{mg} \tag{C.11}$$

$$d_{bo} = S \sin\theta \tag{C.12}$$

Where

F_w — Force exerted by wind per unit length, in N/m

F_m — Weight of the conductor per unit length, in N/m

m — Mass of the conductor, per unit length, in kg/m

g — Acceleration due to gravity, 9.81 m/s^2

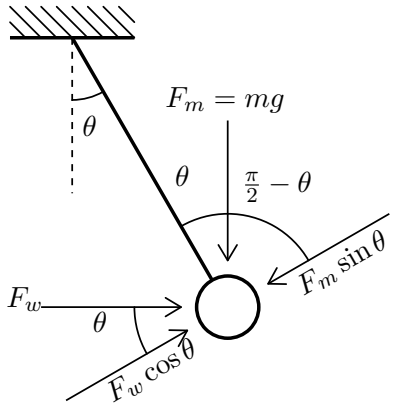

Figure C.5 Blowout Pendulum Model

θ — Blowout angle

S — Total sag distance of span, under given windloaded conditions, in m

More detailed models of conductor blowout can include the length, cross-section, and weight of insulators as well.

Example

A 200-MW transmission line with nominal voltage of 161-kV is constructed with ACSR 'Dove' 556.5-kcmil conductors. The sag distance of the conductor is 15-ft. Find the conductor blow-out for a wind speed of 90-mph, given:

$$d = 0.927in \tag{C.13}$$

$$w = 0.766lb/ft \tag{C.14}$$

The imperial version of C.8 is:

$$P = 0.00256V^2 \tag{C.15}$$

$$F_w = P\frac{d}{12}C_f \tag{C.16}$$

Where

P — **Pressure, in** lbs/ft^2

V — **Wind speed, in** mi/hr

F_w— **Force due to wind, in** lbs

d — **Diameter of conductor, in** in

C_f— **Force coefficient, usually assumed to be 1.0 for stranded conductors**

$$P = 0.00256(50)^2 = 20.74 lbf/ft^2$$

$$F_w = \frac{0.927}{12} 20.74 = 1.602 lbf$$

$$\theta = \arctan \frac{F_w}{w} = \arctan \frac{0.494}{0.766} = 32 \deg$$

$$d_{bo} = 10 \sin 32 \deg = 5.4 ft$$

Blowout due to gusts will likely be accompanied by some differential motion. Conductors will not all blow out to the same distance, with the same speed, or at the same time, due to the variability of wind across time and space. Two conductors in the same plane may not be affected to the same degree as each other - especially if the leading phase causes significant turbulence in the wind stream. Differential motion refers to the speed and distance of the displacement of one conductor in reference to the other. Analytical and experimental studies have shown that, in general, the magnitude of differential displacement between two phases in a transmission line will usually be less than 10% of the magnitude of blowout[108] [109].

C.2.2.2 Partial Ice Loading and "Jumping"

Ice loading of conductors impacts their sag, reducing phase-to-ground clearance. It is also important to look at the effect of unequal ice loading between phases. Unequal ice loading can cause one phase to sag close to another, decreasing the phase-to-phase spacing. A typical calculation will assume maximum ice loading on one strand, an error distance between calculated sag and in-service final sag, and no ice loading on the strand below. Under these assumed static conditions, the distance between phase conductors must be greater than the acceptable withstand distance for a maximum switching surge.

If a significant amount of ice is suddenly shed from a conductor, it's elasticity will cause it to "jump". These jumps can be very large - up to 10 feet vertically, in some cases. Care should be taken to maintain vertical conductor spacing, even in cases of unequal ice loading

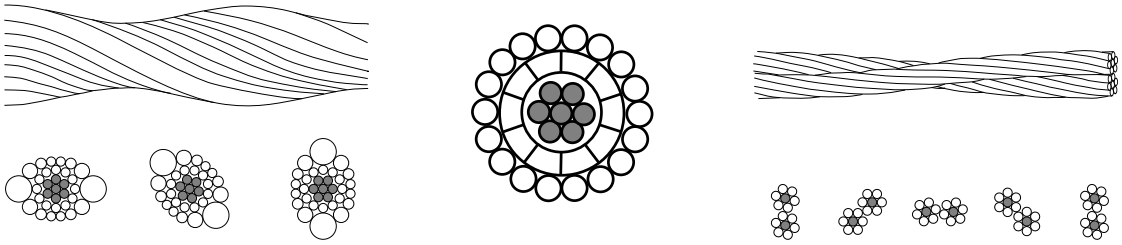

Figure C.6 Oval Vibration-Resistant Cable [111]
, GTACSR Gap-Type Self-damping Conductor [112], and T2 Conductor [113]

and jumping behavior. Research on this phenomena was done on a test line in Saratoga, New York, and jump calculations are presented as a series of empirical curves and correction factors in EPRI's first book on compact line design [104]. Jumping is not as significant an issue in more traditional transmission designs, where phases are arranged horizontally.

C.2.2.3 Vibration

Conductor vibration can occur with lines of any form factor, so it is a well-studied set of phenomena. There are several varieties of conductor vibration which can occur. Vibration is caused by wind, and can change significantly in character, depending on temperatures and ice cover.

Aeolian Vibration is a resonant oscillation caused by vortex shedding by a conductor exposed to a steady wind [104]. This resonanace has a magnitude approximately the width of the conductor, and a frequency of 2-150 Hz. It only occurs for a specific range of tensions and wind speeds. Vibration of this type will cause wear at suspension points, and shorten the life of the structure. This does not significantly impact phase-to-phase clearance, but it may preclude high-tension installations, limiting span lengths. Methods of mitigating this vibration include limiting conductor tension, use of self-damping conductors such as GTACSR, T2, or oval conductors [92], and use of energy-dissipating dampers [104]. Several types of vibration-resistant conductors are shown in C.6. Vibration-resistant conductors dissipate the energy of vibration or break up the uniform flow of wind over the wire [110].

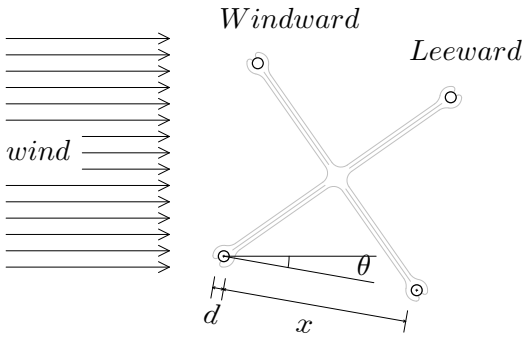

Figure C.7 A 4-Conductor bundle, with tilt angle and spacing parameters identified

Wake-induced Oscillation (WIO) occurs when turbulent air, disrupted by a windward conductor, causes oscillation of a conductor in its wake - diagramed in Figure C.7. Oscillations are several conductor-diameters wide and 1-3 Hz - the natural frequency modes of span conductors. Like Aeolian Vibration, WIO is unacceptable, since its violent motion causes excess wear and mechanical damage. WIO occurs only if the gap between conductors is small, so it has been observed most often on EHV lines with bundled conductors [114]. Conductor spacing ($\frac{x}{d}$, horizontal distance between conductors, over their diameter) is used to describe the boundaries for this type of motion. Phase-to-phase conductor spacing ratios are typically much higher than 30, so WIO is not an issue. WIO most often occurs for conductors with spacing ratios of 10-15. Bundled subconductors are typically spaced less than 18" apart, and often fall into this range. WIO occurs more often in bundles with more than two subconductors, and only occurs when leeward subconductors lie within a narrow range of angles relative to the windward conductor. Methods for reducing WIO include adjusting the tilt of bundles out of the $5^o - 15^o$ range, increasing phase-to-phase spacing ratios $\frac{x}{d}$, and reducing effective spanlengths through the effective use of subconductor spacers.

Galloping is violent large-scale conductor motion caused by unequal wind pressure over the length of a span. This occurs most often when there is ice build up and strong steady wind[114]. Galloping motion is primarily vertical in direction, with magnitudes that can be very large - on occasion, meeting or exceeding the total sag distance of a conductor. Since many new compact

lines are vertically oriented, galloping may be a limiting factor in designing phase-to-phase spacing. Spacing phases too close in the vertical plane may result in excessive phase-to-phase flashovers. T2 conductors (alternately called "VR") conductors are specifically designed to mitigate galloping. These are pairs of smaller conductors, twisted together over wide distances. Under strong winds, these cables will twist as the conductors move. This twisting constantly changes the amount of surface-area exposed to wind, and tends to dissipate kinetic energy more widely across the span, damping vibrations. T2-type conductors may cause increased corona over other conductor alternatives, and so may themselves limit the phase spacing of the line. Other measures to limit galloping include specialized midspan interphase spacers and a variety of novel measures which effectively detune the conductor's vibrating mode.

C.2.3 Right of Way

Phase spacing can impact the Right of Way (ROW) required for a transmission line. ROW is the area leased or purchased by a transmission line owner in order to build a transmission line. ROW easements must be acquired for the entire length of a line. Acquring ROW can be difficult, as it requires transmission developers to acquire permission from dozens of landowners and neighbors. Limiting the amount of required ROW is desirable. Narrower lines are often less visually and physically obtrusive, so land owners are more likely to be accepting of easements on their property. Lines with decreased ROW will also fit in more places, which opens up more options for route designers. Developers must pay for ROW easements, so decreasing ROW can save on costs as well.

ROW width can be limited by a variety of factors. Traditionally, calculation of necessary ROW included the entire width of transmission line structure, space to accomodate natural conductor motion, and a buffer zone — based on voltage flashover clearance or limits on EM field levels[104]. This is demonstrated in Figure C.8.

A minimum ROW width, limited only by flashover distance, can be calculated as follows:

$$L_{ROW} = L_o + 2 \cdot (L_b + L_{buff}) \tag{C.17}$$

Where

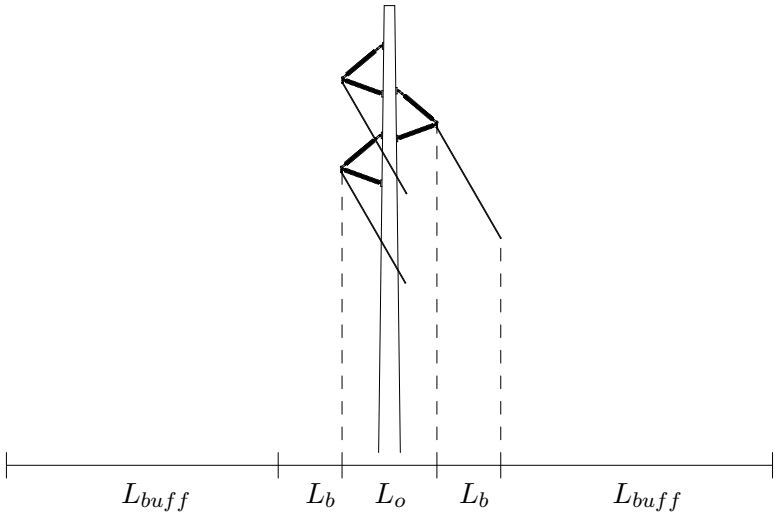

Figure C.8 Right of Way Requirements

L_o — Lateral distance between two most outer conductors

L_b — Blowout distance for a given conductor or set of conductors, as calculated in (C.12)

L_{buff} Buffer zone, here representing the minimum required conductor-to-obstacle flashover withstand defined by the NESC or calculated in (C.5) through (C.7)

The arrangement and decreased phase spacing of compact lines often produce weaker electric and magnetic fields than traditional lines. These lines may require less ROW width in order to limit the electric and magnetic field levels at the edges of the easement. Nominal limits of these fields have been established, based on proven physiological effects [115]. But the scientific literature on extended human exposure to low-level electric and magnetic fields from overhead power lines have not conclusively demonstrated long-term risks [92]. Field limits based on safety considerations will be discussed in a more detailed manner in C.3.2.

Vertically oriented transmission lines clearly present the narrowest physical profile, and often the lowest field levels. One of the most common transmission designs is vertical steel-pole construction. Other common designs include single-pole delta designs and specialized lattice structures with delta arrangements of lines. Most compact designs require less ROW than traditional horizontal arrangements.

C.3 Corona, Audible Noise, Radio Interference, and other Electromagnetic Field Issues

Phase spacing and transmission line geometry will impact the electric fields formed by a transmission line. High electric field gradients can cause corona, audible noise (AN), radio-frequency interference (RI), and losses. Traditionally, these effects have primarily been seen in the design of EHV and UHV lines. But, phase compaction in lower voltage lines can cause levels of electric fields that are as high as older EHV lines. As with most aspects of compact line design, the corona and electric field considerations are not fundamentally different than considerations placed on traditional line designs. But the narrower phase spacing causes factors that previously only affected EHV lines to impact lines at lower voltage.

Corona is a partial discharge resulting from the ionization of air near the surface of a conductor [116]. It occurs only when the voltage stress of the air dielectric rises above a critical level. Corona causes a variety of undesireable environmental effects, including audible noise, radio and television frequency interference, and real power losses ("corona losses"). Excessive noise or interference will prompt complaints from landowners and those living near transmission lines, so it is desireable to minimize these effects. High electric fields can also damage insulators and other structural equipment, which can decrease reliability and increase maintenance costs.

Historically, the public has raised concerns over the levels of electric and magnetic fields to which nearby landowners and neighbors may be subjected. There is little evidence of longterm health effects due to these fields, but some practical limits have been established which account for safety from known physiological effects.

C.3.1 Corona Onset Factors

Corona occurs when the voltage gradient at an electrode rises above a critical level, and gas molecules in the air become stripped of their electrons. This process releases UV light, which is thought to dislodge further electrons from the gas. This process cascades outward from the electrode until the conditions are not sufficient to cause further ionization. These cascades produce streamers of ionized gas and UV light. The ionization produces audible noise as well

as ultra-wideband radio noise [117].

Corona occurs near electrodes with high electric field gradients. Conductors act as electrodes, and their arrangement can be used to increase or decrease gradient levels at conductor surfaces. Large diameter conductors tend to increase the AN and RI, irrespective of their surface gradients. Their larger diameter tends to create electric fields that do not decay as quickly with distance - causing ionization further from the surface of the conductor. The number of bundled conductors will also increase AN generated by a line [118].

Surface conditions of conductors are influential on the level of corona. Conductors covered in dust and polutants are frequently noted to have higher levels of AN and EMI, as are conductors with pitted or irregular surfaces [118]. Hydrophobic surfaces, under wet conditions, also tend to be noisy - due largely for the tendancy of water to collect as droplets and streamers, which create an unven surface over which to spread the instantaneous charge. Low air density also tends to increase corona.

Irregularly shaped clamps and other hardware can cause an irregular charge build-up and excessive localized field gradients. Grading rings are often used on conductor clamps in order to smooth out the electric field and prevent corona from forming. Inappropriate or incorrectly-installed hardware is the source of 90% of complaints from the public, so use of correct hardware is essential.

Corona onset gradient is often estimated from Peek's formula - an empirical formula developed in the 1920s using copper conductors at < 150kV. Peek's formula is [119]:

$$E_C = E_0 m \delta \left[1 + \frac{0.301}{\sqrt{\delta r}}\right] \tag{C.18}$$

$$\delta = \frac{273 + t_0}{273 + t} \cdot \frac{p}{p_0} \tag{C.19}$$

Where

E_C — Minimum peak gradient for visual onset of corona, in kV/cm

E_0 — Gradient breakdown strength of air, Peek estimated this as $29.8 kV/cm$

m — Conductor surface factor, unitless

δ — Relative air density

r — Conductor radius, in cm

t, t_0 — Air temperature in ^oC, and reference air temperature 25^oC

p, p_0 — Air pressure in mm, and reference air pressure $760mm$

If conductors are corroded or contaminated, local corona may occur on the conductor surface even at low gradient levels. But, Peek's formula indicates an approximate gradient at which corona becomes visible – glowing and emitting streamers. The accuracy of this equation depends heavily on selecting an appropriate surface factor m. New clean conductors will have m values around 0.88-0.96, older conductors with some weathering will have values around 0.68-0.82, and wet conductors will have values as low as 0.12-0.23 [120]. It should be clear that corona will be a much more significant factor in wet weather.

The author of [92] suggests that most high-voltage transmission lines have surface field gradients that do not exceed $17kV_{rms}/cm = 24kV_{peak}/cm$. ABB's switchgear manual suggests that most lines will not have fair-weather field gradients above $16 - 19kV_{rms}/cm$, though some may be as high as $21kV_{rms}$.

C.3.2 Calculating Electric and Magnetic Field Magnitudes

Transmission line geometry may be limited by electric and magnetic field limits. Strong electric fields can cause corona, which creates excess AN and RI, and which incurs real losses. In addition, both electric and magnetic fields should be limited in order to account for health concerns. A whole chapter could be written describing the calculation of these fields, but that is not the purpose of this chapter. Instead, a practical estimation method is presented for both electric and magnetic fields. The reader is directed towards [] and [] for further study on the calculation of electric fields, and [] for the calculation of magnetic fields.

The field gradient at the surface of a conductor can be described by several metrics. The maximum field gradient is the highest level of field gradient observed at the surface of a single conductor or subconductor. The maximum bundle gradient is the highest gradient among all the maximum gradients within a bundle. The average-maximum bundle gradient refers to

a simple average of the maximum field gradients of the subconductors in a bundle. For the calculation of corona phenomena, average-maximum bundle (AMB) gradient is used to describe the surface gradient for one phase of the line.

ABB's Switchgear Manual suggests the following method, which calculates the maximum RMS surface gradient for any subconductor in a 3-phase horizontally spaced transmission line with radially symetric bundles and no shield wires. It is closely based on a well-accepted method devised by Markt and Mangele [121].

$$E_{rms} = \frac{V_{rms}}{\sqrt{3}} \cdot \frac{1 + (n-1)r/R}{nr \ln \dfrac{2HD}{r_e\sqrt{4H^2 + D^2}}} \tag{C.20}$$

$$r_{eq} = \left(nrR^{n-1}\right)^{1/n} \tag{C.21}$$

Where

E_{rms} — Maximum subconductor RMS field gradient, in $kV_{rms}/m = 100 \times kV_{rms}/cm$

V_{rms} — Phase-to-phase RMS line voltage, in kV

H — Geometric mean height of conductors, in m

D — Geometric mean distance between centers of phase bundles, in m

r_{eq} — Equivalent radius of a conductor with the same capacitance as a bundle, in m

r — Subconductor radius, in m

n — Number of subconductors in the bundle

R — Bundle radius, in m

Height H is based on mean span height — typically taken to be 1/3 of the distance between maximum sag and the suspension point. Peak values of field gradient E_{rms} are equal to $E_{peak} = \sqrt{2} \cdot E_{rms}$. This gradient value should be kept well below the corona onset gradient, and may be further limited by audible noise or radio interference considerations.

Electric fields must also be measured at ground level at locations far from transmission lines — for instance, when designating ROW width. One of the bases used to limit electric fields is human safety. Electric fields can cause discomforting experiential phenomena in humans. Some

	E-field strength E (kV_{rms} / m)	Magnetic field strength H (A / m)	Magnetic flux density B (μ T)
Occupational	8.33	800	1000
Public	4.17	160	200

Table C.3 ICNIRP suggested exposure limits for 60-Hz non-ionizing radiation

subjects have reported perception of electric fields as low as $2-5kV/m$, with annoyance noted for some subjects in the $15-20kV/m$ range. High levels of electric fields may cause sparking on metallic objects. At higher levels, fields can cause measureable stimulation of peripheral nerve fibers. There is well-established evidence of electric and magnetic fields coupling with magnetic phosphenes in human retinas, causing a perception of visual flickering. Taking all human effects into account, organizations such as the ICNIRP have prescribed limits on human exposure to electric and magnetic fields. Table C.3 lists one set of those limits for 60 Hz [115]. These generally represent levels of exposure well below those that have been associated with measured phenomena, to account for unknown levels of perceptive variation among humans. Safety levels are linked to immediate phenomena, which can be documented and measured, not any long-term effects. In the ICNIRP guidelines, it is noted that there is no conclusive evidence linking low-frequency non-ionizing radiation with cancer rates or long-term health risks.

To present the calculation of electric fields far from a transmission line, we must dig a little deeper into the methodology of calculating electric fields, but again, the method of derivation is not the emphasis here - simply, the breif demonstration of a known method. A transmission line is modeled as a set of parallel line charges with densities Q_k expressed as complex quantities in coulombs/meter. Each of these lines has a known potential V_k, a phasor with real and imaginary parts expressed in volts. The ground plane has an assumed potential of 0. In order to account for this uniform ground potential, a set of 'image' charges are defined such that for each conductor in the line with charge Q_k at height H_k, a conductor of opposite charge $-Q_k$ exists at height $-H_k$. With these mirrored charges, the potential of the ground is zero everywhere, and all field lines enter the ground perpendicularly, as we should expect. Shield wires and other grounded conductors are included, with potentials of zero. At each line k, the

sum of potentials due to the other charges $Q_1, Q'_1, Q_2, Q'_2 ..., Q_k, Q'_k, ...Q_N, Q'_N$ must be equal to its own voltage V_k. The potential at line k due to line l is related by P_{kl}, known as Maxwell's coefficient of potential. Coefficients of potential are equal to:

$$P_{kk} = \frac{1}{2\pi\epsilon_0} \ln\left(\frac{2H_k}{r_k}\right) \tag{C.22}$$

$$P_{kl} = \frac{1}{2\pi\epsilon_0} \ln\left(\frac{D'_{kl}}{D_{kl}}\right) \tag{C.23}$$

Where

P_{kk} — Self potential coefficient, in m/F

P_{kl} — Mutual potential coefficient, in m/F

r_k — Radius of conductor k, in m

H_k — Height above ground of conductor k, in m

D_{kl} — Distance from conductor k to conductor l, in m

D_{kl} — Distance from conductor k to image conductor l, in m

If bundles exist and are arranged in radial symmetry, they can be reduced to equivalent conductors located at their bundle centers, with radii calculated as in (C.21). The relationship between charges $[Q]$, potentials $[V]$, and potential coefficients $[P]$ is known to be $[Q] = [P]^{-1}[V]$. Solve for Q. These charges can be used to calculate the electric field at a point H_m meters above ground level X_m meters from the center of the line, using the following formulae:

$$\tilde{E}_{kx} = \frac{\tilde{Q}_k}{2\pi\epsilon_0} \cdot \left[\frac{x_m - x_k}{(x_m - x_k)^2 + (h_k - h_m)^2} - \frac{x_m - x_k}{(x_m - x_k)^2 + (h_k + h_m)^2}\right] \tag{C.24}$$

$$\tilde{E}_{ky} = \frac{\tilde{Q}_k}{2\pi\epsilon_0} \cdot \left[\frac{h_m - h_k}{(x_m - x_k)^2 + (h_k - h_m)^2} - \frac{h_m + h_k}{(x_m - x_k)^2 + (h_k + h_m)^2}\right] \tag{C.25}$$

$$E_{rms} = \sqrt{|\sum_k \tilde{E}_{kx}|^2 + |\sum_k \tilde{E}_{ky}|^2} \tag{C.26}$$

Where

E_{rms} — Magnitude of total electric field at measurement point (X_m, H_m)

$\tilde{E}_{kx}$ — Lateral component of the complex field gradient due to charge k

$\tilde{E}_{kx}$ — Vertical component of the complex field gradient due to charge k

x_m — Lateral coordinate of measurement

x_k — Lateral coordinate of charge k

h_m — Vertical coordinate of measurement

h_k — Vertical coordinate of charge k

The level E_{rms} should be kept below whatever reference level is considered necessary. If the most limiting reference level is human safety according to the ICNIRP, then E_{rms} should be set below the public level (4.17 kV_{rms} / m) at the edge of the ROW. Electric fields at the edge of ROW can be reduced by decreasing phase spacing and minimizing the number of subconductors used. Increasing conductor height will also reduce electric field strength.

Magnetic field levels should also be calculated for the edge of the ROW, to assure public safety and compliance. Like electrical fields, magnetic field strength can be decreased by reducing phase spacing and increasing conductor height. Magnetic fields should also be set below safe limits.

Magnetic field levels are comparatively simple to calculate. The following formulae can be used to calculate the magnetic field level at a point H_m meters above ground level X_m meters from the center of the line:

$$\tilde{B}_{kx} = \frac{\mu_0 \mu_r \tilde{I}_k}{2\pi} \cdot \frac{h_m - h_k}{(x_m - x_k)^2 - (h_m - h_k)^2} \tag{C.27}$$

$$\tilde{B}_{ky} = \frac{\mu_0 \mu_r \tilde{I}_k}{2\pi} \cdot \frac{x_k - x_m}{(x_m - x_k)^2 - (h_m - h_k)^2} \tag{C.28}$$

$$B_{rms} = \sqrt{|\sum_k \tilde{B}_{kx}|^2 + |\sum_k \tilde{B}_{ky}|^2} \tag{C.29}$$

Example:

A 345kV transmission line is to be built with horizontal phase spacing. Bundles are 2-954 kcmil ACSR, with diameter 1.196" and spacing of 18". Phases are spaced 24' apart, with a suspended height of 50' and a 20' average sag. The line is rated at 1200 MW. Find the maximum surface field gradient, and the electric and magnetic field levels 5' off the ground 30' from the outside phase — representing the head of a person standing on the edge of a ROW.

1a) Maximum surface field gradient

Find the mean conductor height H, the height 1/3 the distance between suspended height and sagged height. Also find r_{eq}.

$$H = [(50 - 20) + (1/3) \cdot 20]36.67ft$$

$$r_{eq} = \left(nrR^{n-1}\right)^{1/n} = \left(2 \cdot (1.196/2) \cdot (18/2)^{2-1}\right)^{1/2} = 3.281"$$

Convert other measures to m.

r = (1.196/2)" = 0.0152 m = 1.52 cm

R= (18/2)" = 0.229 m

H= 36.67' = 11.18 m

D= $(18 \cdot 18 \cdot 36)^{1/3}$= 9.217 m

r_{eq}= 3.281" = 0.0833 m

Now, calculate E_{rms}

$$E_{rms} = \frac{345}{\sqrt{3}} \cdot \frac{1 + (2-1)0.0152/0.229}{2 \cdot 0.0152 \ln \frac{2 \cdot 11.18 \cdot 9.217}{r_e\sqrt{4 \cdot 11.18^2 + 9.217^2}}} = 1511kV/m = 15.11kV/cm$$

Check the corona onset gradient for a weathered conductor m=0.7, and δ=1.

$$E_{C,rms} = (E_0/\sqrt{2})m\delta\left[1 + \frac{0.301}{\sqrt{\delta r}}\right] = (29.8/\sqrt{2}) \cdot 0.7 \cdot 1\left[1 + \frac{0.301}{\sqrt{1 \cdot 1.52}}\right] = 18.35kV/cm$$

Maximum conductor surface gradient is still well below corona onset.

1b) Calculate E-field at the measurement point

First, calculate [P], from (C.22) and (C.23). r_{eq} should be the same as above.

$$P = \frac{1}{2\pi\epsilon_0}\begin{bmatrix} \ln\left(\frac{2H}{r_{eq}}\right) & \ln\left(\frac{D'_{12}}{D_{12}}\right) & \ln\left(\frac{D'_{13}}{D_{13}}\right) \\ \ln\left(\frac{D'_{12}}{D_{12}}\right) & \ln\left(\frac{2H}{r_{eq}}\right) & \ln\left(\frac{D'_{23}}{D_{23}}\right) \\ \ln\left(\frac{D'_{13}}{D_{13}}\right) & \ln\left(\frac{D'_{23}}{D_{23}}\right) & \ln\left(\frac{2H}{r_{eq}}\right) \end{bmatrix} = \begin{bmatrix} 10.05 & 2.10 & 1.08 \\ 2.10 & 10.05 & 2.10 \\ 1.08 & 2.10 & 10.05 \end{bmatrix} \times 10^{10}$$

Now, calculate the charges at each phase, based on $\tilde{V}$. $\tilde{V}$ is a phasor of phase-to-ground voltage at each phase.

$$[\tilde{Q}] = [P]^{-1}[\tilde{V}] = 10^{-10} \cdot \begin{bmatrix} 10.05 & 2.10 & 1.08 \\ 2.10 & 10.05 & 2.10 \\ 1.08 & 2.10 & 10.05 \end{bmatrix}^{-1} \begin{bmatrix} \frac{345}{\sqrt{3}}\angle 0^o \\ \frac{345}{\sqrt{3}}\angle 120^o \\ \frac{345}{\sqrt{3}}\angle 240^o \end{bmatrix} = \begin{bmatrix} 2.365 \times 10^{-6}\angle 5.59^o \\ 2.557 \times 10^{-6}\angle 240^o \\ 2.365 \times 10^{-6}\angle 114.41^o \end{bmatrix}$$

Finally, calculate E_{kx} and E_{ky} for each phase, and calculate E_{rms}. Utilizing (C.24 - C.26) results in the following:

$$E_x = \begin{bmatrix} 144.0\angle 5.59^o \\ 327.5\angle 240^o \\ 611.8\angle 114.41^o \end{bmatrix}, \; E_y = \begin{bmatrix} 1366.4\angle 185.59^o \\ 2568.8\angle 60^o \\ 4525.9\angle 294.41^o \end{bmatrix}, \; E_{rms} = 2738V/m = 2.738kV/m$$

1c) Calculate the magnetic field at the measurement point

The nominal current in each phase is $|I| = 1200MW/345kV/\sqrt{3} = 2008.2A$. Now, calculate each B_{kx} and B_{ky}, and find $|B_{rms}|$. Utilizing (C.27 - C.29) yields:

$$B_x = \begin{bmatrix} 145.0\angle 0^o \\ 181.6\angle 120^o \\ 207.8\angle 240^o \end{bmatrix} \mu T, \; B_y = \begin{bmatrix} 58.9\angle 180^o \\ 106.5\angle -60^o \\ 219.3\angle 60^o \end{bmatrix}, \; \mu T B_{rms} = 152.8\mu T$$

In Figure C.9, the E and B fields at head level have been calculated for several variations on the transmission line in the example above. The black dotted line indicates the ICNIRP public

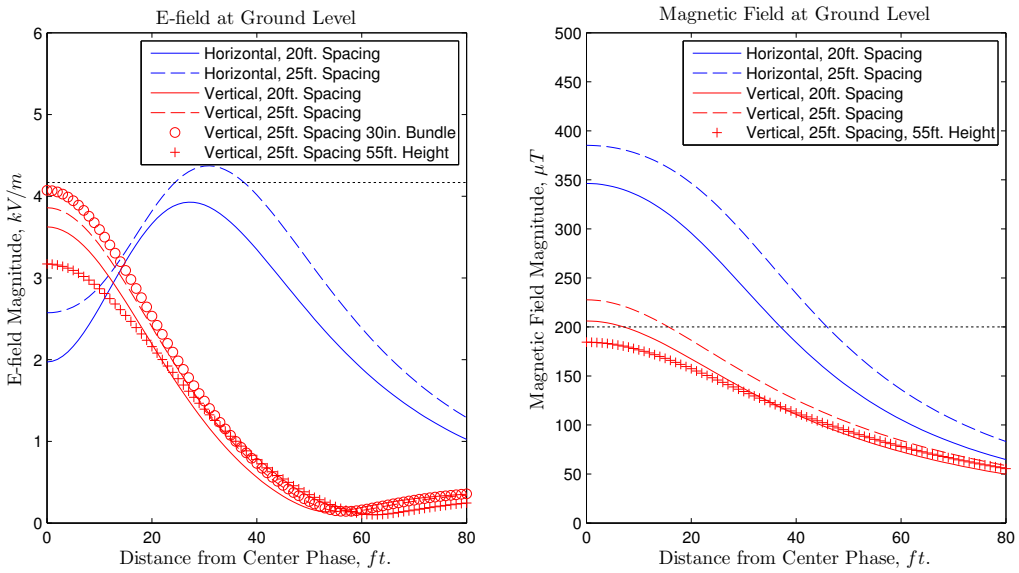

Figure C.9 Electric and magnetic fields at a height of 5', for variations of the example problem

exposure reference limit for each value. Notice that both fields are significantly less intense for the lines with vertical phase spacing. The fields cancel more evenly, since the absolute distance from the measurement point to the conductors is less uneven, and the absolute distance from the measurement location to the conductors is greater. These lines will be significantly taller than the traditional horizontally spaced line. But, they cover less lateral space, and their EM field performance is far less limiting than that of horizontal lines. Increasing bundle spacing will significantly increase electric field levels near the lines. Notice also that raising the line just 5 feet significantly decreases both electric and magnetic fields.

C.3.3 Audible Noise

Audible noise caused by corona should be considered in the design of compact lines. Corona causes high-frequency broadband noise, as well as humming at harmonics of the fundamental power-frequency. The broadband noise is caused primarily by corona streamers, while the hum is caused by surface corona. High levels of noise will not be tolerated by neighbors or other landowners. Corona noise will be most significant during wet or rainy weather — often, the only time that a line exhibits corona is during poor weather. In fair weather, for the most part,

lines will operate at well below the corona onset gradient voltage.

Noise ordinances may differentiate between wet and fair weather noise limits. Limits may also differentiate between daytime and nighttime noise levels, with nighttime levels being more stringent. Noise ordinances specify allowable noise levels as statistical measures of A-weighted sound pressure. A-weighting is an approximation of human perception of noise levels — a summation of perceived loudness over a wide range of audible frequencies — and is the commonly used measure of environmental noise. Noise limits are measured from the edge of a ROW. Noise ordinances vary significantly by location, but many are based on EPA guidelines set out in 1974 which suggest the following long-term-average outdoor noise limits[122]:

$$L_{dn} \leq 55dBA \text{ or}$$

$$L_{eq(24)} \leq 55dBA \tag{C.30}$$

$$L_{dn} = L_{eq} + 10dBA \tag{C.31}$$

$$L_{eq(24)} = 10 \log \frac{1}{24} \left[\sum_{i \in d} 10^{L_{eq,i}} + \sum_{i \in n} 10^{L_{dn,i}} \right] \tag{C.32}$$

Where

L_{eq} — Equivalent long-term average noise level, over a single hour, in dBA

L_{dn} — Equivalent noise level during night-time hours (typically, 10:00 PM to 7:00 AM), in dBA

$L_{eq(24)}$ — Equivalent long-term average noise level over 24 hours, in dBA

d — Index of daytime hours

n — Index of nighttime hours

In (C.30), L_{dn} is used as a limit for residential areas, farmyards, and places where people may spend large parts of their day. $L_{eq(24)}$ is suggested as a limit for places that are more infrequently occupied. Nighttime noise levels are given a $10dBA$ adder to account for the greater potential for noise to become an annoyance at night. The EPA report notes that background noise levels

at night are typically much lower, so noises that would not be perceptible during daytime hours become more pronounced at night. L_{dn} is an hourly limit, and is more restrictive than $L_{eq(24)}$ which is weighted average. Since rainy and wet conditions can occur at any hour of the day, and corona noise is typically highest during rainy periods, many lines are designed to meet the more restrictive L_{dn} limit, rather than the normal daytime limit L_{eq}. If a line is designed to meet the 24-hour average limit, $L_{eq(24)}$ should be calculated with rainy noise levels replacing several of the night-time hours.

Audible noise levels can be approximated by a variety of methods. One oft-cited empirical method was derived by engineers at Bonneville Power Administration, based on long-term statistical data from a number of test lines. They suggest that noise levels during measurable rain can be calculated [123]:

$$L_{eq,i} = -164.6 + 120 \log_{10} E_i + 55 \log_{10} d_{e,i} \tag{C.33}$$

$$L_{eq} = 10 \log_{10} \left\{ \sum_{i=1}^{n} \exp[0.23(L_{eq,i} - 11.4 \log_{10} D_i - 5.8)] \right\} \tag{C.34}$$

$$d_e = \begin{cases} d, & \text{if } n \leq 2 \\ 0.58 \cdot n^{0.48} \cdot d, & \text{n} > 2 \end{cases} \tag{C.35}$$

Where

$L_{eq,i}$ — Noise potential of phase i, in dBA

L_{eq} — Audible noise for all phases, in dBA

E_i — Maximum voltage gradient at phase i, in kV_{rms}/cm

$d_{e,i}$ — Equivalent diameter of conductor i, in mm

d — Diameter of conductor, in mm

D_i — Distance from measurement location to point i, in m

Corona noise during fair weather is hard to predict, since corona is often non-existent. However, during hot summer months, lines can exhibit significant corona and noise. Observe that when operating at high temperatures (for high-temperature conductors this may be 100^oC

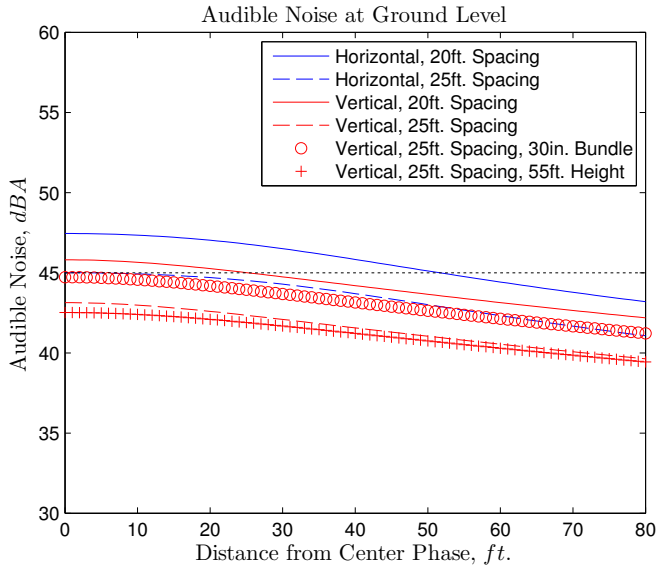

Figure C.10 Audible noise at a height of 5', for variations of the example problem

or higher), air density will drop according to (C.19), and corona onset may occur at lower gradient levels. BPA suggests that fair-weather noise of a line is typically 25dBA below the noise level with measureable rain.

In Figure C.10, audible noise levels have been calculated according to the BPA method for several variations of the line listed in the previous example problem. Notice again that a vertical phase arrangement decreases audible noise levels. Wide bundle spacing and narrow phase spacing both appear to increase noise levels. As before, a small increase in tower height also leads to preferable outcomes. Though not pictured here, increasing conductor size will also lead to significant decreases in audible noise.

C.3.4 Radio and Television Interference

Corona produces significant broadband radio- and tv-frequency interference noise (RI and TVI). As with audible noise, RI and TVI are most severe during rainy weather — when corona most often occurs. However significant RI has been noted, even during fair weather. Observations suggest that in foul weather, RI can increase by 20dB [124] — enough to cause perceptible static.

TVI is most significant for rural residents. Typically, VHF and UHF signals are very strong, and even significant noise does not cause noticible degredation. But, for rural customers with high-gain directional antennas, sporatic cases of interference have been known to occur. As noted previously, most corona issues are caused by improper or badly-installed hardware, not line geometry. Often, disturbances of this kind can be remedied by repairing or replacing badly performing hardware.

Radio noise tends to increase with decreased phase spacing, and increases with decreased conductor size. It is not significantly affected by the number of subconductors in a bundle. Radio noise is most strongly affected by the nearest phase to the observer [118].

The IEEE Radio Noise Design group has published design guides on industry practices to reduce radio and TV interference [124]. EPRI has published detailed models for calculating expected interference at a variety of frequencies [125].

C.3.5 Corona Losses

Corona activity results in losses in real power. High voltage gradients rip electrons off gas molecules, producing ions and UV light, and displacing ions. This consumes energy and produces an added irregular power draw from the conductors. In poor weather conditions, when corona occurs, these losses can be nearly equal to resistive losses. But, on an annual average, losses are very slight - often orders of magnitude less than resistive losses.

Corona losses can be estimated, according to empirical formulae. One such formula, based on data from a BPA test line, is given in (C.36) [117]. This formula is appropriate for calculating corona loss in poor weather:

$$P_{dB} = 14.2 + 65\log_{10}\left(\frac{E_m}{18.8}\right) + 40\log_{10}\left(\frac{d}{3.51}\right) + K_1 \cdot \log\left(\frac{n}{4}\right) + K_2 + \frac{A}{300} \tag{C.36}$$

$$K_1 = \begin{cases} 13, & \text{n} \leq 4 \\ 19, & \text{n} > 4 \end{cases}$$

$$K_2 = \begin{cases} 10 \cdot \log_{10}\left(\frac{RR}{1.676}\right), & \text{RR} \leq 3.6 \\ 3.3 + 3.5 \cdot \log_{10}\left(\frac{RR}{3.6}\right), & \text{RR} > 3.6 \end{cases}$$

Where

P_{dB} — Per-phase losses, in dB above $1W/m$

n — Number of subconductors

d — Diameter of each subconductor, in cm

E_m — Maximum average maximum gradient of subconductors in bundle, in kV/cm

RR — Rain rate, in mm/hr

A — Altitude, in m

Per-mile 3-ϕ corona losses can be calculated:

$$P_{3-\phi} = 1609.4 \cdot \sum_{i=1}^{3} 10^{P_{dB,i}/10}, \tag{C.37}$$

where $P_{dB,i}$ is the decibal corona loss at phase i and $P_{3-\phi}$ is the 3-phase losses in W/mi. This same study suggests, based on observations of a test line, that to calculate average losses during fair weather, subtract 17dB from the average losses during rainy weather.

C.4 Increased Loadability due to High Surge-Impedence Loading designs

Transmission line loadability can be increased through the use of designs with increased surge impedence loading levels. Compact transmission lines, with their generally narrower phase-to-phase distances, tend to have lower surge impedence and thus higher Surge-Impedence Loading (SIL) values than traditional transmission lines. This is especially important for Extra-High-Voltage (EHV) lines (345kV and up) which tend to be built over longer distances and require greater reactive control. Long transmission lines designed with lower surge impedence tend to support greater stable transfers of power.

This section will first describe increase SIL can lead to higher line ratings, then it will investigate the phenomena that lead to lower Surge Impedence.

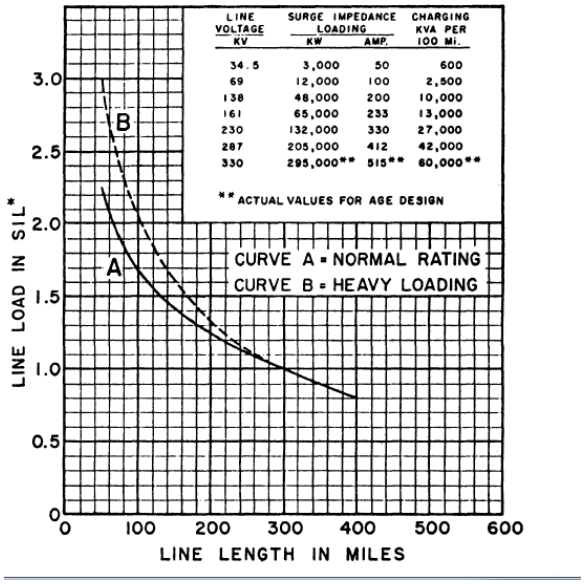

Figure C.11 St. Clair's Loadability Curves

C.4.1 The Effect of High Surge Impedence Loading on Transmission Line Rating

Several factors will determine the rating of a transmission line. Short lines are limited most severely by physical restrictions - the sag of conductors at high temperatures, costly losses, or EM field levels. Resistive losses are the main contributor to physical constraints. These are easily reduced through the use of larger conductors, or a larger number of conductors. Thermal constraints are mostly independent of line length, since they do not measure total losses, only the temperature at every point along the line. Longer lines tend to be limited by voltage drop limits and angular stability limits. These will be length-dependant, as the quantities that they limit will increase with line length (voltage drop is nearly linear with reactance, as is angular separation). These are influenced primarily by reactive losses, which can be reduced, but not as simply or substantially as can resistive losses. Empirical studies and years of experience have shown transmission designers that the transfer limit of a line generally follows the same curve – called a St. Clair curve – based on SIL and total line length. A typical St. Clair curve is shown in Figure C.11 [126]. Note that voltage and angle stability only become limiting factors for lines longer than 50 or 100 miles. Lower voltage transmission lines are rarely impacted by these limitations, since they are not typically used for long-distance transfers.

Compact lines, due to their typically-narrower phase-to-phase distances, tend to have lower surge impedances, and thus higher SIL levels than traditional line configurations. In some cases, lines have been designed explicitly with this in mind [127] [128]. As previously mentioned, some line ratings may be increased by utilizing designs with higher SIL. A variety of geometrical variations can be exploited to increase SIL.

C.4.2 Surge Impedence Loading

Surge Impedence is the natural impedence of a transmission line. Surge Impedence Loading (SIL) is the MW power transfer level at which reactive power required to support the magnetic field of the line is balanced by capacitive power produced by the line's electric field. At this level, reactive losses of the line are canceled out and only resistive losses occur.

A distributed parameter model of a transmission line can be described by the following terminal equations [129]:

$$V_1 = V_2 \cosh \gamma l + Z_c I_2 \sinh \gamma l \tag{C.38}$$

$$I_1 = I_2 \cosh \gamma l + \frac{V_2}{Z_c} \sinh \gamma l \tag{C.39}$$

$$Z_c = \sqrt{\frac{z}{y}} \tag{C.40}$$

$$\gamma = \sqrt{yz} \tag{C.41}$$

Where

V_1, V_2 — Voltage at the source and sink terminals, a phasor, in V

I_1, I_2 — Current at the source and sink terminals, a phasor, in A

Z_c — Surge impedence (or "characteristic impedance"), a phasor, in Ω

γ — The propogation constant, a phasor, in Ω

z — Per-phase series impedence per distance, in complex Ω/mi

y — Per-phase shunt admittance per distance, in complex Ω/mi

l — Line length, in mi

For a line of given length l, this model can be converted to a PI-model lumped-circuit equivalent with shunt admittance Y' and series impedence Z' as shown in Figure **??**. It can be shown that the parameters of this model circuit are equal to the following [129]:

$$Z' = Z_c \sinh \gamma l = zl \frac{\sinh \gamma l}{\gamma l} \tag{C.42}$$

$$\frac{Y'}{2} = \frac{1}{Z_c} \tanh \frac{\gamma l}{2} = \frac{yl}{2} \frac{\tanh(\gamma l/2)}{\gamma l/2} \tag{C.43}$$

For transmission lines less than around 100 miles long, $\frac{\sinh \gamma l}{\gamma l} \simeq 1$, and $\frac{\tanh(\gamma l/2)}{\gamma l/2} \simeq 1$. For these lines, $Z' = zl$ and $\frac{Y'}{2} = \frac{yl}{2}$ are close approximations.

Surge impedance loading (SIL) occurs when the load driven by the line matches the natural impedance of the line itself. A line with surge impedence of Z_c serving power to a bus of voltage V will have a nominal SIL of:

$$P_{SIL} = V \left(\frac{V}{Z_c} \right)^* = \frac{VV^*}{Z_c^*} = \frac{|V|^2}{Z_c^*} \tag{C.44}$$

Example:

A 345 kV transmission line 200 miles long has a per-phase reactance of $0.7656\Omega/mi$**, resistance of** $0.068\Omega/mi$**, and capacitive admittance of** $5.548 \times 10^{-6} j\Omega^{-1}/mi$**. Find this line's surge impedence, SIL, and PI-equivalent parameters** Z' **and** $\frac{Y'}{2}$**.**

$$\begin{aligned}
Z_c &= \sqrt{\frac{z}{y}} && = 371.82 - j1.65 \ \Omega \\
P_{SIL} &= \frac{|V|^2}{Z_c^*} && = 319.49 - j14.15 \ MVA \\
\gamma &= \sqrt{yz} && = 9.14 \times 10^{-5} + j2.063 \times 10^{-3} \ \Omega \\
Z' &= zl \frac{\sinh \gamma l}{\gamma l} && = 12.83 + j148.85 \ \Omega \\
\frac{Y'}{2} &= \frac{yl}{2} \frac{\tanh(\gamma l/2)}{\gamma l/2} && = 7.217 \times 10^{-7} + j5.628 \times 10^{-4} \ \Omega^{-1}
\end{aligned}$$

Test the approximations:

$$\begin{aligned}
Z' &\simeq zl && = 13.59 + 153.11 \ \Omega \\
\frac{Y'}{2} &\simeq \frac{yl}{2} && = 0 + j5.548 \times 10^{-4} \ \Omega^{-1}
\end{aligned}$$

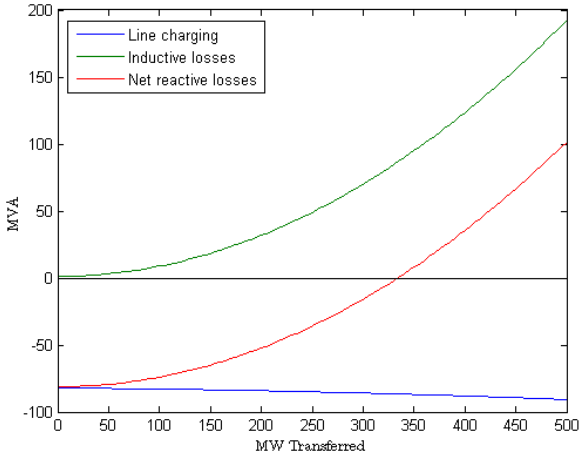

Figure C.12 Reactive Power Contributions

Reactive losses tend to drag down line voltage and increase angular separation across a line. These two effects can make heavily-loaded lines unstable [127]. If a line has a high SIL, it will have natural reactive support at higher loading levels, resulting in less severe voltage drops across the line.

In the following demonstration, a 345kV line, as described in the previous example, is modeled at varying levels of delivered power P_2. The transfer is assumed to have unity power factor ($S_2 = P_2$) and receiving end voltage V_2 of 1.0 p.u. Figure C.12 shows the reactive power consumption of the transmission line. Notice that the total reactive power consumed crosses 0 near 319MW - that is, near the nominal P_{SIL} rating. Above that level, reactive losses increase rapidly. Figures C.13 and C.14 show sending end voltage magnitude V_1 and the angular separation of the sending and receiving buses Θ_1 and Θ_2. Not surprisingly, large transfers contribute to significant voltage drops and angular separations.

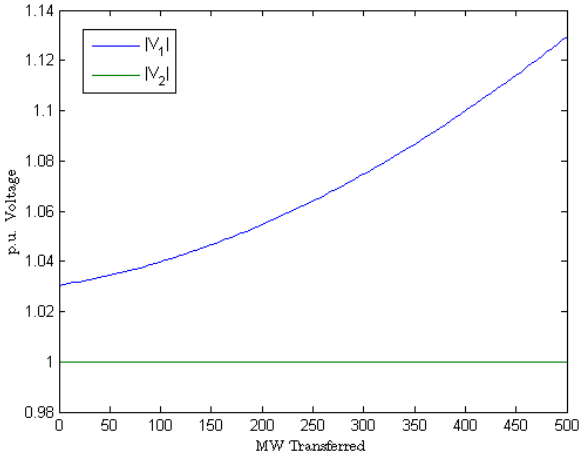

Figure C.13 Terminal Voltages V_1 and V_2

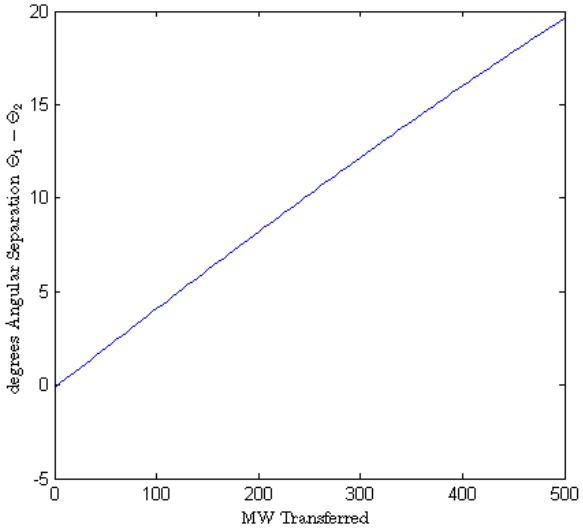

Figure C.14 Angular Separation $\Theta_1 - \Theta_2$

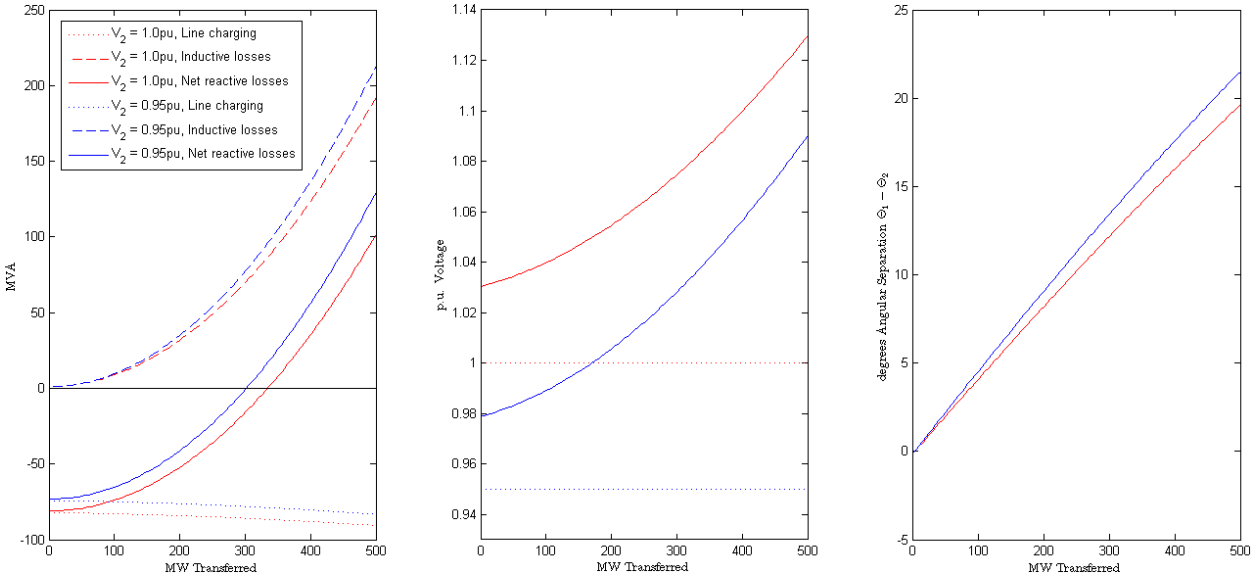

Figure C.15 Reactive Losses, Terminal Voltages, and Angular separation, for $V_2 = 1.0$p.u. and $V_2 = 0.95$p.u.

Due to a variety of operational states, net reactive consumption of a line may not be precisely zero at a transfer level of $P = P_{SIL}$. Voltage drops and angular separation will be exasperated by lower terminal voltages. Lowering the line voltage decreases the capacitive VARs generated by the line while increasing the current necessary to deliver power. Both of these effects increase the net reactive consumption of the line. This effect is demonstrated in Figure C.15. A lower receiving-end power factor will require greater absolute line current, and thus higher real and reactive losses. The strength of the connected system may also impact reactive losses and voltage levels [126]. A line with higher SIL will have generally better loadability than if the same line were built with a lower SIL. But, two separate lines with the same SIL may behave differently, depending on their context within the larger grid.

C.4.3 The Effect of Narrow Phase-Spacing and Bundle Geometry on Surge Impedence Loading

Surge impedance is calculated based on two properties - series impedance z and shunt admittance y. Impedance z is composed of resistance and inductance. Resistance is dependent on conductor materials, and does not change significantly with line geometry. Typically, resistance

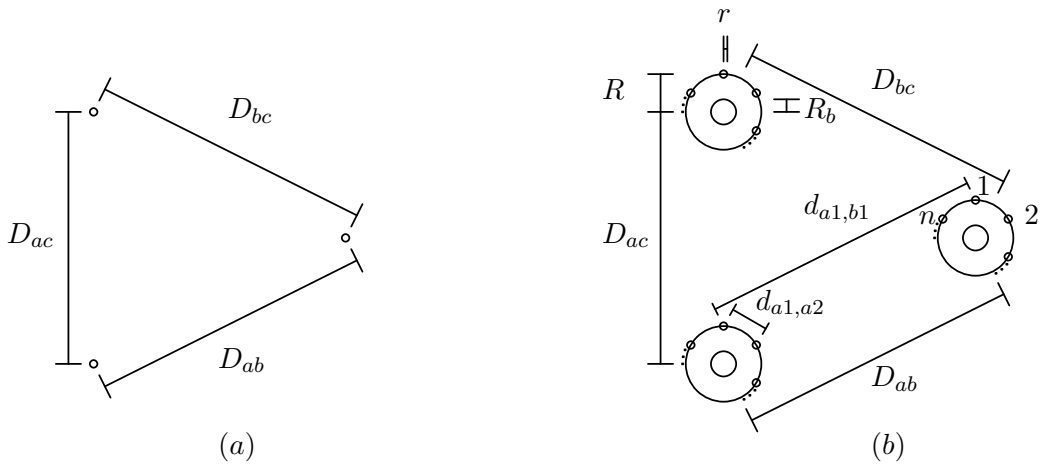

Figure C.16 Dimensions for (a) 3-Phase Conductor Arrangement (b) 3-Phase Conductor Arrangement with Bundles of n Subconductors

is minimal compared to inductive reactance. Inductance depends strongly on coupled magnetic fields which are quite dependent on line geometry. Shunt admittance is modeled as a capacitive admittance, and is also impacted by line geometry. To discern the effects of geometry on surge impedance, the series inductance and capacitive admittance of a line are investigated separately in this section.

C.4.3.1 Series Inductive Reactance

The reactance of a transmission line measures the coupling of magnetic fields caused by current flowing in the conductors. The primary geometric parameters that impact a line's series reactance are the Geometric Mean Distance (GMD) between phases conductors, and the Geometric Mean Radius (GMR) of the bundled conductors.

A transmission line with geometry outlined in Figure C.16(a) has an average per-phase flux-linkage-per-meter that can be accurately approximated:

$$\lambda_a = \frac{\mu_0}{2\pi}\left[i_a \ln\frac{1}{r'} + i_b \ln\frac{1}{D} + i_c \ln\frac{1}{D}\right] \tag{C.45}$$

$$r' = re^{-\mu_r/4} \tag{C.46}$$

$$D = (D_{ab}D_{bc}D_{ac})^{1/3} \tag{C.47}$$

Where

λ_a — Average a-phase flux-linkage per meter of line, in H/m

In a balanced line, $\lambda_a = \lambda_b = \lambda_c$

D — Geometric mean distance between phases, in m

μ_0 — $4\pi \times 10^{-7} \frac{H}{m}$, Permeability of free space

r — External radius of a solid cylindrical conductor, in m

r' — Radius of an equivalent hollow cylindrical conductor with the same flux linkage as a solid conductor with radius r, in m

μ_r — Relative permeability of conductor material. For non-magnetic materials such as Aluminum, typically $\mu_r \simeq 1$

n — Number of subconductors in each bundle

D_{ab}— Distance from phase-a conductors to phase-b conductors, in m

This equation is relatively accurate for balanced 3-phase transmission lines with periodic transposition, for which $D >> r$. Observe that as the distance between phase conductors decreases, the magnetic couplings of all phases are strengthened. If the currents on this line are balanced and separated by 120^o, $i_a + i_b + i_c = 0$, or $-i_a = i_b + i_c$. By substitution, we can see that:

$$\lambda_a = \frac{\mu_0}{2\pi}\left[i_a \ln\frac{1}{r'} + (i_b + i_c)\ln\frac{1}{D}\right] = \frac{\mu_0}{2\pi}\left[i_a \ln\frac{1}{r'} - i_a \ln\frac{1}{D}\right] = \frac{\mu_0}{2\pi}\left[i_a \ln\frac{D}{r'}\right] \tag{C.48}$$

Clearly, as flux-linkage between phases are strengthened, self-linkage of each individual phase is partially canceled by the combined linkage from the other two phases. Since reactance $x = \omega L = \omega\frac{\lambda}{i}$, a decrease in flux will result in a decrease in inductive reactance x. So, decreasing the average spacing between phases results in decreased series-reactance on the line.

A transmission line with multiple bundled conductors on each phase, as shown in Figure C.16(b), can be represented in a manner very similar to that of a non-bundled transmission

line. The generalized flux linkages for conductor $a1$ will be equal to:

$$\begin{aligned}\lambda_{a1} = \frac{\mu_0}{2\pi}[&i_{a1}\ln\frac{1}{r'} + i_{a2}\ln\frac{1}{d_{a1,a2}} \quad ... + i_{an}\ln\frac{1}{d_{a1,an}} \\ &+i_{b1}\ln\frac{1}{d_{a1,b1}} \quad ... + i_{bn}\ln\frac{1}{d_{a1,bn}} \\ &+i_{c1}\ln\frac{1}{d_{a1,c1}} \quad ... + i_{cn}\ln\frac{1}{d_{a1,cn}}]\end{aligned} \tag{C.49}$$

where n is the number of subconductors per phase, and $d_{ai,bj}$ is the distance from subconductor ai to subconductor bj. Assume that phase current is split equally between all subconductors ($i_{a1} = ... = i_{an} = \frac{i_a}{n}$). Equation C.49 becomes:

$$\lambda_{a1} = \frac{\mu_0}{2\pi}[i_a\ln\frac{1}{R_b} + i_b\ln\frac{1}{D_{a1,b}} + i_c\ln\frac{1}{D_{a1,c}}] \tag{C.50}$$

Where

$$\begin{aligned}R_b &= (r'd_{a1,a2}...d_{a1,an})^{1/n} \\ D_{a1,b} &= (d_{a1,b1}d_{a1,b2}...\ d_{a1bn})^{1/n} \\ D_{a1,c} &= (d_{a1,c1}d_{a1,c2}...\ d_{a1cn})^{1/n}\end{aligned}$$

R_b is known as the Geometric Mean Radius (GMR) of the bundle. If bundles are radially symetric and identical for all phases, R_b will be identical for each subconductor. Notice that since intra-bundle distances (e.g. $d_{a1,a2}$) are much smaller than inter-bundle distances (e.g. $d_{a1,b1}$), it is reasonable to suggest that $D_{a1,b} \simeq D_{ab}$ and $D_{a1,c} \simeq D_{ac}$. Equation C.50 becomes:

$$\lambda_{a1} = \frac{\mu_0}{2\pi}\left[i_a\ln\frac{1}{R_b} + i_b\ln\frac{1}{D_{ab}} + i_c\ln\frac{1}{D_{ac}}\right], \tag{C.51}$$

which looks very much like (C.49). If we assume as before that the phase currents are balanced, and that the line is periodically transposed, we again have:

$$\lambda_{a1} = \lambda_{a1} = \frac{\mu_0}{2\pi}\left[i_a\ln\frac{D}{R_b}\right] \tag{C.52}$$

A single subconductor, then, will have inductance $L_{a1} = \frac{\lambda_{a1}}{i/n} = \frac{n\lambda}{ni} = \frac{\lambda}{i}$. Since D and R_b are approximately equal for all subconductors in a bundle, and subconductors are connected

in parallel, the per-phase reactance of a bundled transmission line will be approximately:

$$x = \omega L \simeq \omega \frac{1}{n \times \frac{i}{n\lambda_{a1}}} \simeq \omega \frac{\mu_0}{2\pi} \ln \frac{D}{R_b} \tag{C.53}$$

If intra-bundle spacing decreases, R_b decreases and x will increase. This is the opposite of what was seen with the decrease in phase spacing. This occurs because all bundled conductor currents are in phase with each other. Bringing bundled subconductors closer together increases magnetic flux coupling in phase with their self-inductance, intensifying rather than cancelling out the fields of other subconductors.

Thus, both decreasing phase-phase spacing and increasing bundle spacing will have the effect of decreasing series reactance x.

Example

A 345kV transmission line in horizontal configuration has phase-to-phase spacing of $D_{ab} = 26'$, $D_{bc} = 26'$, and $D_{ac} = 52'$. It is strung with 2-conductor bundles of 954.0 kcmil "Rail" conductors (diameter = 1.165"), $18''$ apart. a) Find the reactance-per-mile of this line. b) Find the reactance-per-mile if phase-to-phase spacing were reduced to $23'$. c) Find the reactance-permile if bundle spacing were increased to 24". d) Find the reactance-per-mile if the bundles were replaced with 3 636.0 kcmil "Rook" conductors (diameter = $.977''$) arranged equilaterally 18" apart.

a) Reactance per mile of original line

$$D = (D_{ab}D_{bc}D_{ac})^{1/3} = 32.76ft = 9.985m$$

$$r' = re^{-\mu_r/4} = (1.165in/2) * e^{-1/4} = .4537in = 0.0115m$$

$$R_b = (r'd)^{1/2} = (.4537in * 18in)^{1/2} = 2.8577in = 0.0726m$$

$$x = \omega \frac{\mu_0}{2\pi} \ln \frac{D}{R_b} = 60(2\pi) \frac{4\pi \times 10^-7}{2\pi} \ln \frac{9.985}{0.0726} = 0.0003713\Omega/m = 0.5975\Omega/mi$$

b) Reactance-per-mile for $23'$ spacing

$$D = (D_{ab}D_{bc}D_{ac})^{1/3} = (23 * 23 * 46)^{1/3} = 28.98ft = 8.833m$$

$$x = \omega \frac{\mu_0}{2\pi} \ln \frac{D}{R_b} = 60(2\pi) \frac{4\pi \times 10^-7}{2\pi} \ln \frac{8.833}{0.0726} = 0.0003202\Omega/m = 0.5826\Omega/mi$$

c) Reactance-per-mile for 24" bundle spacing

$$D = (D_{ab} D_{bc} D_{ac})^{1/3} = (26 * 26 * 52)^{1/3} = 32.76ft = 9.985m$$

$$R_b = (r'd)^{1/2} = (.4537in * 24in)^{1/2} = 3.2996in = 0.0838m$$

$$x = \omega \frac{\mu_0}{2\pi} \ln \frac{D}{R_b} = 60(2\pi) \frac{4\pi \times 10^-7}{2\pi} \ln \frac{9.985}{0.0838} = 0.0003604\Omega/m = 0.5801\Omega/mi$$

d) Reactance-per-mile for 3-conductor bundle

$$D = (D_{ab} D_{bc} D_{ac})^{1/3} = (26 * 26 * 52)^{1/3} = 32.76ft = 9.985m$$

$$r' = re^{-\mu_r/4} = (0.977in/2) * e^{-1/4} = .3804in = 0.00966m$$

$$R_b = (r'd)^{1/2} = (.3804in * 18in * 18in)^{1/3} = 4.977in = 0.1264m$$

$$x = \omega \frac{\mu_0}{2\pi} \ln \frac{D}{R_b} = 60(2\pi) \frac{4\pi \times 10^-7}{2\pi} \ln \frac{9.985}{0.1264} = 0.0003294\Omega/m = 0.5302\Omega/mi$$

C.4.3.2 Capacitive Admittance

The capacitive admittance of a transmission line measures the strength of the electric field formed between conductors of differing potentials. The primary geometric parameters used to calculate this phenomena are also the line-to-line GMD and the GMR of bundled conductors. The GMR used for calculation of capacitance is defined slightly differently than the GMR used in the inductive reactance calculations.

A 3-phase transmission line with geometry outlined in Figure C.16(a) will have an approximate potential of:

$$v_a = \frac{1}{2\pi\epsilon} \left(q_a \ln \frac{1}{r} + q_b \ln \frac{1}{D_{ab}} + q_c \ln \frac{1}{D_{ac}} \right) \tag{C.54}$$

Where

v_a — Surface voltage of a-phase conductor, in V

q_a — Charge per meter on conductor a, in coulombs/meter

ϵ — Dielectric permittivity, typically close to $\epsilon_0 = 8.8542... \times 10^{-12} F/m$, permittivity in a vacuum

D_{ab}— Distance from phase-a conductors to phase-b conductors, in m

If this line is transposed periodically, (C.54) becomes:

$$v_a = \frac{1}{2\pi\epsilon}\left(q_a \ln\frac{1}{r} + q_b \ln\frac{1}{D} + q_c \ln\frac{1}{D}\right) \tag{C.55}$$

Where

$D = (D_{ab}D_{ac}D_{bc})^{1/3}$, the GMD phase-to-phase spacing

If we assume that $q_a + q_b + q_c = 0$ (physically, that the area near the line is at net-neutral charge and the only displaced charges are those on the line's conductors), then (C.55) becomes:

$$v_a = \frac{1}{2\pi\epsilon}\left(q_a \ln\frac{1}{r} - q_a \ln\frac{1}{D}\right) = \frac{1}{2\pi\epsilon} q_a \ln\frac{D}{r} \tag{C.56}$$

Since capacitance is defined by the relationship $c = \frac{q}{v}$, and v_a represents the phase-to-neutral voltage of the line, the per-phase phase-to-neutral capacitance per meter of this line is:

$$c = \frac{2\pi\epsilon}{\ln(D/r)} \tag{C.57}$$

Notice that if the GMD is decreased, capacitance increases. This may be understood by refering back to (C.55). If D is decreased, charges q_b and q_c are both brought closer to charge q_a, and the electric field formed by each charge has a stronger effect on the other charges. Since $q_a = -(q_b + q_c)$, the electric fields due to the combination of q_b and q_c will tend to cancel out the field due to q_a. So, as these charges are brought closer together, they partially cancel out each others' fields. Since potential v_a is the integral of electric field strength, the potential due to a point charge q_a is decreased. Now, a greater charge q will be required to form potential v. Capacitance $c = \frac{q}{v}$ is therefore increased. Capacitive admittance b is equal to $b = \omega c$, so a decrease in GMD increases capacitive admittance.

Bundled conductors, shown in Figure C.16(b), can be represented in a similar fasion. The generalized representation of the potential at point p in space due to charges at points

$a1...an, b1..., bn, c1..., cn$ is given by:

$$\begin{aligned} v_p = \frac{1}{2\pi\epsilon}(q_{a1}\ln\frac{1}{r} \quad & +q_{a2}\ln\frac{1}{d_{a1,a2}}... + q_{an}\ln\frac{1}{d_{a1,an}} \\ +q_{b1}\ln\frac{1}{d_{a1,b1}} \quad & +q_{b2}\ln\frac{1}{d_{a1,b2}}... + q_{bn}\ln\frac{1}{d_{a1,bn}} \\ +q_{c1}\ln\frac{1}{d_{a1,c1}} \quad & +q_{c2}\ln\frac{1}{d_{a1,c2}}... + q_{cn}\ln\frac{1}{d_{a1,cn}}) \end{aligned} \tag{C.58}$$

Where

v_p — Potential at point p

q_{ai} — Charge per meter on subconductor i of phase a, in coulombs/meter

$d_{ai,bj}$ Distance between the centers of subconductor i of phase a and subconductor j of phase b, in m

It should be apparent that the distance between subconductors of different phases (e.g. $d_{ai,bj}$) will be very close to the distances between bundle centers (e.g. D_{ab}). With that approximation, (C.58) becomes:

$$\begin{aligned} v_{a1} \simeq \frac{1}{2\pi\epsilon}(q_{a1}\ln\frac{1}{r} + q_{a2}\ln\frac{1}{d_{a1,a2}}... + q_{an}\ln\frac{1}{d_{a1,an}} \\ +q_b\ln\frac{1}{D_{ab}} + q_c\ln\frac{1}{D_{ac}}) \end{aligned} \tag{C.59}$$

Where

D_{ab} — Distance between centers of bundles a and b, in m

q_b — Total charge per meter of subconductors $q_{b1}, q_{b2}...$, and q_{bn}: $q_b = q_{b1} + q_{b2}... + q_{bn}$

The potential due to charges q_b and q_c is nearly equal for all subconductors in bundle a. The potentials on each subconductor of phase a should be nearly equal to each other ($v_{a1} = v_{a2}... = v_{an}$), since they are all energized to the same voltage. If another subconductor potential, is substituted in (i.e. $v_{a1} = v_{ai}$), it is clear, the potential due to other a-phase subconductor charges is the same for all subconductors in a phase. If bundles are radially symmetric, it can also be shown that each subconductor position is simply a transposition of the first subconductor, so the effect of other subconductor charges on its potential will be equal. This suggests that all subconductor charges in a phase will be equal to each other

($q_{a1} = q_{a2}... = q_{an} = \frac{q_a}{n}$). Thus, for a transmission line with radially symmetric bundles, the potential at $a1$ can be expressed:

$$v_{a1} = \frac{1}{2\pi\epsilon}(q_a \ln \frac{1}{R_b^c} + q_b \ln \frac{1}{D_{ab}} + q_c \ln \frac{1}{D_{ac}}) \tag{C.60}$$

Where

q_a — Total charge per meter of subconductors $q_{a1}, q_{a2}...$, and q_{an}: $q_a = q_{a1} + q_{a2}... + q_{an}$

R_b^c— Geometric Mean Radius for capacitive calculations, $R_b^c = (rd_{a1,a2}...d_{a1,an})^{1/n}$

If, as before, we assume that all charges sum to zero, and that the line undergoes periodic transposition, (C.60) becomes:

$$v_{a1} = \frac{1}{2\pi\epsilon}(q_a \ln \frac{D}{R_b^c}) \tag{C.61}$$

Where

D — Geometric Mean Distance between bundles, $D = (D_{ab}D_{ac}D_{bc})^{1/3}$

The per-phase phase-to-neutral capacitance per meter of this bundled line is:

$$c = \frac{2\pi\epsilon}{\ln(D/R_b^c)} \tag{C.62}$$

Observe that if subconductor bundle spacing is increased (R_b^c is larger), capacitance c is also increased. Since all subconductors in a bundle have approximately the same charge (thus, the same polarity), the fields they produce will be complementary. Increasing bundle spacing reduces the complementary effect of these fields, decreasing the field strength and increasing the charge q_a due to potential v_a.

Thus, both decreasing phase-to-phase spacing and increasing bundle spacing will have the effect of increasing capacitive admittance b.

Example

The same transmission line as the previous example is to be built. a) Find the capacitive admittance-per-mile of this line. b) Find the equivalent capaci-

tive reactances of a 100-mile stretch of this line. c) Find the admittance-per-mile if phase-to-phase spacing were reduced to $23'$. d) Find the capacitance and admittance-per-mile if bundle spacing were increased to $24"$. e) Find the capacitance and admittance-per-mile if the bundles were replaced with 3 636.0 kcmil "Rook" conductors (diameter $= .977''$) arranged equilaterally $18"$ apart.

a) Capacitance and admittance per mile of original line

$$D = (D_{ab}D_{bc}D_{ac})^{1/3} = 32.76ft = 9.985m$$

$$r = (1.165in/2) = .5825in = 0.0148m$$

$$R_b^c = (rd)^{1/2} = (.5825in * 18in)^{1/2} = 3.2381in = 0.0822m$$

$$b = \omega\frac{2\pi\epsilon}{\ln D/R_b^c} = 60(2\pi)\frac{2\pi 8.854\times10^{-12}}{\ln\frac{9.985}{0.0822}} = 4.370\times10^{-9}\Omega^{-1}/m = 7.033\times10^{-6}\Omega^{-1}/mi$$

b) Capacitive reactance in equivalent model

$$\frac{Y'}{2} \simeq \frac{yl}{2} = \frac{j7.033\times10^{-6}\Omega^{-1}/mi\times100mi}{2} = j351.6\times10^{-6}\Omega^{-1}$$

$$|X_{Y'/2}| = \frac{1}{Y'/2} = \frac{1}{351.6\times10^{-6}\Omega^{-1}} = 2844.3\Omega$$

c) Capacitance and admittance-per-mile for $23'$ spacing

$$D = (D_{ab}D_{bc}D_{ac})^{1/3} = (23*23*46)^{1/3} = 28.98ft = 8.833m$$

$$b = \omega\frac{2\pi\epsilon}{\ln D/R_b^c} = 60(2\pi)\frac{2\pi 8.854\times10^{-12}}{\ln\frac{8.833}{0.0822}} = 4.485\times10^{-9}\Omega^{-1}/m = 7.218\times10^{-6}\Omega^{-1}/mi$$

d) Capacitance and admittance-per-mile for $24"$ bundle spacing

$$D = (D_{ab}D_{bc}D_{ac})^{1/3} = (26*26*52)^{1/3} = 32.76ft = 9.985m$$

$$R_b^c = (rd)^{1/2} = (.5825in * 24in)^{1/2} = 3.739in = 0.0950m$$

$$b = \omega\frac{2\pi\epsilon}{\ln D/R_b^c} = 60(2\pi)\frac{2\pi 8.854\times10^{-12}}{\ln\frac{9.985}{0.0950}} = 4.505\times10^{-9}\Omega^{-1}/m = 7.251\times10^{-6}\Omega^{-1}/mi$$

e) Capacitance and admittance-per-mile for 3-conductor bundle

$$D = (D_{ab}D_{bc}D_{ac})^{1/3} = (26*26*52)^{1/3} = 32.76ft = 9.985m$$

$$r = (0.977in/2) = .4885in = 0.0124m$$

$$R_b^c = (rd^2)^{1/2} = (.4885in * 18in * 18in)^{1/3} = 5.4092in = 0.1374m$$

$$b = \omega\frac{2\pi\epsilon}{\ln D/R_b^c} = 60(2\pi)\frac{2\pi 8.854\times10^{-12}}{\ln\frac{9.985}{0.1374}} = 4.8933\times10^{-9}\Omega^{-1}/m = 7.875\times10^{-6}\Omega^{-1}/mi$$

C.4.3.3 Surge Impedence

It was observed that narrowing the phase-to-phase spacing of a line will decrease line reactance x and increase capacitive admittance b. Recall that surge impedence is defined as:

$$Z_c = \sqrt{\frac{r + jx}{jb}}$$

A decrease in x and increase in b will result in a lower Z_c. Decreased surge impedence equates to higher SIL, so a narrowing of phase spacing leads to an increased SIL. Increasing bundle spacing also decreases reactance and increases capacitance. Thus, both narrowing phase spacing and widening bundle spacing will increase the line's surge impedence loading.

Increasing the number of subconductors in a bundle is also an effective method of raising SIL. This increases the GMR of bundles. The average distance between subconductors increases, which decreases flux coupling of in-phase currents and decreases complementary electric fields for in-phase voltages. This method may be expensive, however, as it adds complexity and extra parts to the design.

Example: Find the surge impedence and SIL of the 345kV line and its variants described in the previous two sections. Assume that resistive losses are negligible.

a) 2-conductor 18" bundles, 26' apart

$$Z_c = \sqrt{\frac{r + jx}{jb}} = \sqrt{\frac{0 + j0.5975\Omega/mi}{j7.033 \times 10^{-6}\Omega^{-1}/mi}} = 291.5\Omega$$

$$P_{SIL} = 3\frac{|V_{p-n}|^2}{Z_c} = 3\frac{(345,000/\sqrt{3}V)^2}{291.5\Omega} = 408.4MVA$$

b) 2-conductor 18" bundles, 23' apart

$$Z_c = 284.1\Omega$$

$$P_{SIL} = 419.2MVA$$

c) 2-conductor 24" bundles, 26' apart

$$Z_c = 282.8\Omega$$

$$P_{SIL} = 420.8MVA$$

d) 3-conductor 18" bundles, 26' apart

$$Z_c = 259.5\Omega$$

$$P_{SIL} = 458.7MVA$$

Assymetrical bundle shapes can also be employed to decrease surge impedence and increase SIL [127], relative to symmetrical bundles of the same spacing. In simulations, assymetrical designs have been shown to be more effective than symmetrical designs in reducing SIL. The same principles that reduce reactance and increase capacitance are at work in these designs, but their unique shapes appear to be more effective at reducing self-coupling of magnetic fields and decreasing electric field strengths.

C.5 Conclusion

Compact transmission line design is not fundamentally different from traditional design, but it requires consideration of more factors that were not as important in traditional design. Reduction in phase-to-phase spacing can decrease line noise, decrease ground-level electrical and magnetic fields, decrease required ROW, and increase SIL. On the other hand, decreased phase-to-phase spacing can increase surface gradients on conductors, leading to corona. It requires special designs and hardware to prevent excess flashover due to conductor motion and decreased withstand distances. Widening bundles can increase SIL, but will exasperate groundlevel electric fields. Adding subconductors will usually reduce surface gradients and increase SIL. Increasing conductor size will reduce surface gradients, increase SIL, reduce audible noise (due to decreased corona), and decrease ground-level electric field levels. But, if conductor size is increased and surface gradients are held constant, audible noise will increase.

Phase arrangement is very important. Horizontal phase spacing is rarely used. Vertical spacing leads to significant decreases in ground-level electric fields and magnetic fields, as well as decreasing required ROW and increasing capacitance. However, tall vertical structures are expensive, and may conflict with zoning ordinances or FAA guidelines. Other modern designs include vertical-delta arrangements, which require more ROW than vertical designs but less than horizontal arrangements. Still other more exotic tower arrangements acheive better phase

compaction than vertical designs, though they are not yet common and may be perceived as unsightly. Vertical lines are, by comparison, far more pleasing to the eye and may be more readily accepted by the public.

Compact construction of transmission lines is a design philosophy rather than a set of specific designs. Line compaction is utilized in the design of most new transmission lines.

Bibliography

[1] Iowa Wind Energy Association. Wind power facts, 2013. Accessed 3/11/13.

[2] Energy Information Administration. Electric power monthly - december 2012, December 2012.

[3] Mark Bolinger Ryan Wiser. 2010 wind technologies market report. Technical report, U.S. Department of Energy, August 2011.

[4] Energy Information Administration. Electric power annual 2007 - 2011, January 2013.

[5] U. S. Energy Information Administration. Annual electric generator report: Electric generating capacity, 2013.

[6] Mark Bolinger Ryan Wiser. 2011 wind technologies market report. Technical report, U.S. Department of Energy, August 2012.

[7] North Carolina State University Solar Center. Renewable electricity production tax credit (ptc), 2013. Accessed 3/11/13.

[8] Michigan Public Service Commission. Report on the implementation of the p.a. 295 renewable energy standard and the cost-effectiveness of the energy standards. 2013.

[9] Synapse Energy Economics. The potential rate effects of wind energy and transmission in the midwest iso region, 2012.

[10] North American Electric Reliability Corporation. Potential impacts of future environmental regulations, 2011.

[11] U.S. Department of Energy. 20% wind energy by 2030: Increasing wind's contribution to the us energy supply, July 2008.

[12] U.S. Department of Energy. Eastern wind integration and transmission study, January 2010.

[13] PNM TVA MAPP et. al. Midwest ISO, SPP. Joint coordinated system plan 2008, 2008.

[14] J.A. Fleeman, R. Gutman, M. Heyeck, M. Bahrman, and B. Normark. Ehv ac and hvdc transmission working together to integrate renewable power. In *Integration of Wide-Scale Renewable Resources Into the Power Delivery System, 2009 CIGRE/IEEE PES Joint Symposium*, pages 1–1, July.

[15] T.J. Hammons, D. Woodford, J. Loughtan, M. Chamia, J. Donahoe, D. Povh, B. Bisewski, and W. Long. Role of hvdc transmission in future energy development. *Power Engineering Review, IEEE*, 20(2):10–25, 2000.

[16] Roberto Rudervall, J.P. Charpentier, and Raghuveer Sharma. High voltage direct current (hvdc)transmission systems technology review paper. In *Energy Week 2000*.

[17] World's first 800 kv hvdc link goes into operation in china. *Power Engineering International*, December 2009.

[18] Yao Lei; Jiang Ying; Sun Xinqin; Wang Zheng; Ling Wei; Chang Bingyu.

[19] Jameson T. Smith, Ryan Pulkrabek, Jarred S. Miland, Laura Rauch, Jeanna Furnish, Matt Sutton, Ronghai Wang, and Khurram Ansar. Regional generation outlet study. Technical report, Midwest Independent System Operator, November 2010.

[20] PE Gentile, Thomas J., PhD Elizondo, David C., and PhD Ray, Swakshar. Phase 1 report: Strategic midwest area renewable transmission (smartransmission) study. Technical report, Quanta Technology, July 2010.

[21] Bob Fagan and Max Chang et. al. The potential rate effects of wind energy and transmission in the midwest iso region, May 2012.

[22] MISO Staff. Planning year 2013-2014 wind capacity credit. Technical report, Midwest Independent System Operator, December 2012.

[23] S.; DeMeo E.; Reilly J.M.; Mai T.; Arent D.; Porro G.; Meshek M.; Sandor D. Hand, M.M.; Baldwin. Renewable electricity futures study. Technical report, National Renewable Energy Laboratory, 2012.

[24] Dale Osborn. Hvdc as high capacity overlay. April.

[25] Tore Wizelius. *Developing Wind Power Projects: THeory and Practice*. Earthscan.

[26] Ryan; Porter Kevin Mills, Andrew; Wiser. The cost of transmission for wind energy: A review of transmission planning studies, 2009.

[27] X. Wang and J.R. McDonald. *Modern power system planning*. McGraw-Hill, 1994.

[28] L.L. Garver. Transmission network estimation using linear programming. *Power Apparatus and Systems, IEEE Transactions on*, PAS-89(7):1688–1697, 1970.

[29] Hui Zhang, V. Vittal, G.T. Heydt, and J. Quintero. A mixed-integer linear programming approach for multi-stage security-constrained transmission expansion planning. *Power Systems, IEEE Transactions on*, 27(2):1125–1133, 2012.

[30] M.J. Rider, I. de J.Silva, R. Romero, A.V. Garcia, and C.A. Murari. Transmission network expansion planning in full open market considering security constraints. In *Power Tech, 2005 IEEE Russia*, pages 1–6, 2005.

[31] Hong Fan, Haozhong Cheng, Zhiwei Ying, Fengqing Jiang, and Fangdi Shi. Transmission system expansion planning based on stochastic chance constrained programming with security constraints. In *Electric Utility Deregulation and Restructuring and Power Technologies, 2008. DRPT 2008. Third International Conference on*, pages 909–914, 2008.

[32] I. De J Silva, M.J. Rider, R. Romero, A.V. Garcia, and C.A. Murari. Transmission network expansion planning with security constraints. *Generation, Transmission and Distribution, IEE Proceedings-*, 152(6):828–836, 2005.

[33] Huang Wei, Feng Li, He Zijun, Cui Junzhao, and Zhang Li. Transmission network planning with n-1 security criterion based on improved multi-objective genetic algorithm.

In *Electric Utility Deregulation and Restructuring and Power Technologies (DRPT), 2011 4th International Conference on*, pages 1250–1254, 2011.

[34] Oriol Gomis-Bellmunt, Jun Liang, Janaka Ekanayake, Rosemary King, and Nicholas Jenkins. Topologies of multiterminal hvdc-vsc transmission for large offshore wind farms. *Electric Power Systems Research*, 81(2):271 – 281, 2011.

[35] H. Ergun, D. Van Hertem, and R. Belmans. Transmission system topology optimization for large-scale offshore wind integration. *Sustainable Energy, IEEE Transactions on*, 3(4):908–917, 2012.

[36] Wind Today. Iowa wind farms completed as of march 31, 2010, 2010. Accessed 3/1/2013.

[37] Federal Aviation Administration. Obstruction evaluation off airport cases 1999 - 2011. Electronic Document, 2011.

[38] MidAmerican Energy. Just the facts: Midamerican energy iowa wind-powered electric generation, 2012. Accessed 3/8/2013.

[39] MidAmerican Energy. Midamerican energy company announces completion of 2012 iowa wind projects, 2012. Accessed 3/8/2013.

[40] Dairyland Power Co-operative. Winnebago wind power project (thompson, iowa), 2012.

[41] Alliant Energy. Franklin county wind farm begins producing emissions-free energy, 2012. Accessed 3/8/2013.

[42] Maquoketa Valley Electric Co-operative. Elk wind is iowa's asset, 2012. Accessed 3/8/2013.

[43] Tama-Toledo Chronicle. Cipco adding new iowa-based wind energy, 2012. Accessed 3/8/2013.

[44] Iberdrola. Iberdrola renewables announces ppas with comed and ameren: New harvest wind farm output sold to illinois utilities, 2010. Accessed 3/8/2013.

[45] The Grundy Register. Wellsburg wind farm project back on track, 2012. Accessed 3/8/2013.

[46] Algonquin Power & Utilities Corp. Algonquin power & utilities corp. announces acquisition of 480 mw of wind generation, 2012. Accessed 3/8/2013.

[47] Tradewinds Energy. English farms i wind project, 2012. Accessed 3/8/2013.

[48] AWS Truepower. Iowa - annual average wind speed at 80 m. Electronic Document, 2010. Accessed 6/1/2011.

[49] Iowa Wind Energy Association. Iowa wind farms completed as of march 31, 2010, 2010.

[50] American Wind Energy Association. Awea siting handbook 2008. Electronic Document, 2008. Accessed 3/20/2013.

[51] American Wind Energy Association. In the public interest: How and why to permit for small wind systems, 2008. Accessed 3/20/2013.

[52] Windustry. Community wind toolbox, 2008. Accessed 3/20/2013.

[53] Alameda County Scientific Review Committee. Guidelines for siting wind turbines recommended for relocation to minimize potential collision-related mortality of four focal raptor species in the altamont pass wind resource area, 2010. Accessed 3/20/2013.

[54] Roland B. Stull. *An Introduction to Boundary Layer Meteorology.* Atmospheric Sciences Library. Kluewer Academic Publishers, 1988.

[55] Paul Denholm, Maureen Hand, Maddalena Jackson, and Sean Ong. Land-use requirements of modern wind power plants in the united states. Technical report, National Renewable Energy Laboratory, August 2009.

[56] Story County Planning and Development Department. Story county land development regulations, 2006. Accessed 3/20/2013.

[57] Plymouth County Board of Supervisors. Zoning ordinance, 2006. Accessed 3/20/2013.

[58] Carroll County Zoning Department. Ordinance #14, 2009. Accessed 3/20/2013.

[59] The Grundy County Planning & Zoning Commission. Grundy county, iowa, devlopment ordinance, 2009. Accessed 3/20/2013.

[60] Part 77 — safe, efficient use, and preservation of the navigable airspace. Current as of April 18, 2013.

[61] Wind Easement Work Group. Wind energy easements and leases: Compensation pakages, 2009.

[62] Erin Golden. Iowa town reaps windfall from turbines, 2011.

[63] Windustry. Landowner guide: Evaluating a wind energy development company.

[64] Paul Muncy. Queue process workshop: Generation interconnection. Presented for interested parties at MISO headquarters on October 20, 2011.

[65] Midwest Independent System Operator. Interconnection transmission capacity contour map, February 2012.

[66] Clipper Windpower Development Company. Docket e-21973 petition for electric transmission line franchise, 2009.

[67] Jeremiah Doner. Miso transmission cost allocation overview, 2012. Presented at MISO headquarters July 6, 2012.

[68] U.S. Department of Energy. Guide to purchasing green power, 2010.

[69]

[70] North Carolina State University Solar Center. Financial incentives for renewable energy. Accessed 2/23/2013.

[71] AWS Truepower. State wind resource potential tables. Electronic Document, 2010. Accessed 3/23/2013.

[72] Iowa Department of Natural Resources. Natural resources geographic information systems library, url =.

[73] MidAmerican Energy. Just the facts: 345,000 volt transmission line from council bluffs to grimes. Online, 2003. Accessed 4/2/2013.

[74] Midwest ISO. Multi value project portfolio: Results and analyses. Electronic Document, 2012. Accessed 4/2/2013.

[75] Melissa McHenry. Aep, midamerican transmission joint venture to develop two 765-kv transmission projects in the midwest, 2010. Accessed 4/2/2013.

[76] H.P. St.Clair. Practical concepts in capability and performance of transmission lines. *Power Apparatus and Systems, Part III. Transactions of the American Institute of Electrical Engineers*, 72(2):1152–1157, 1953.

[77] R. Gutman, P.P. Marchenko, and R.D. Dunlop. Analytical development of loadability characteristics for ehv and uhv transmission lines. *Power Apparatus and Systems, IEEE Transactions on*, PAS-98(2):606–617, 1979.

[78] Clean Line Energy Partners. Rock island cleanline: Project description, 2012. Accessed 3/1/2013.

[79] A.J. Wood and B. F. Wollenberg. *Power Generation, Operation and Control*. Wiley, 1984.

[80] Jiachun Guo, Yong Fu, Zuyi Li, and M. Shahidehpour. Direct calculation of line outage distribution factors. *Power Systems, IEEE Transactions on*, 24(3):1633–1634, 2009.

[81] Beth Conley. Technology development: Rock island clean line: Farm to market road for the 21st century. Remarks presented at Iowa Wind Energy Association Conference, March 27, 2013.

[82] Iowa Utilities Board. State of iowa 115-345 kv electric transmission lines. Electronic document, available at request, 2001.

[83] Ken Wicker. Emery generating station, clear lake, iowa. *Power*, July/August 2005.

[84] MidAmerican Energy. Just the facts, 2007.

[85] Energy Information Administration. Electric power annual 2011, January 2013.

[86] E.S. Thayer. Computing tensions in transmission lines. *Electrical World*, 84:72–83, July 12, 1924.

[87] Y. Motlis, J.S. Barrett, G.A. Davidson, D.A. Douglass, P.A. Hall, J.L. Reding, T.O. Seppa, Jr. Thrash, F.R., and H.B. White. Limitations of the ruling span method for overhead line conductors at high operating temperatures. *Power Delivery, IEEE Transactions on*, 14(2):549 –560, apr 1999.

[88] 2012 national electrical safety code (nesc). *National Electrical Safety Code, C2-2012*, pages 1 –389, 1 2011.

[89] H.W. Adams. Steel supported aluminum conductors (ssac) for overhead transmission lines. *Power Apparatus and Systems, IEEE Transactions on*, PAS-93(5):1700 –1705, sept. 1974.

[90] M. Iordanescu, J. Tarnowski, G. Ratel, and R. Desbiens. General model for sag-tension calculation of composite conductors. In *Power Tech Proceedings, 2001 IEEE Porto*, volume 4, page 4 pp. vol.4, 2001.

[91] Ieee standard for calculating the current-temperature of bare overhead conductors. *IEEE Std 738-2006 (Revision of IEEE Std 738-1993)*, pages c1 –59, 30 2007.

[92] F. Kiessling, P. Nefzger, J.F. Nolasco, and U. Kaintzyk. *Overhead Power Lines: Planning, Design, Construction.* Springe-Verlag, Berlin Heidelberg, Germany, 2003.

[93] H. E. House and P. D. Tuttle. Current-carrying capacity of acsr. *Power Apparatus and Systems, Part III. Transactions of the American Institute of Electrical Engineers*, 77(3):1169 –1173, april 1958.

[94] Iec technical report: Overhead line electrical conductors - calculation methods for stranded bare conductors. *IEC TR 61597*, 1995.

[95] Acss. Product Specification Sheet, 2011.

[96] Power Systems Engineering Research Center. Characterization of composite cores for high-temperature low-sag conductors, 2009.

[97] Acsr. Product Specification Sheet, 2011.

[98] Dale A. Douglass. Practical application of high-temperature low-sag (htls) transmission conductrors. Online.

[99] Aluminum conductor composite reinforced (accr) - frequently asked questions.

[100] Tim Kavanagh and Oisin Armstrong. An evaluation of high-temperature low-sag conductors for uprating the 220kv transmission network in ireland. *45th International Universities Power Engineering Conference (UPEC)*, 2010.

[101] J-Power Systems. Gtacsr (gap-type thermal-resistant aluminum alloy steel reinforced) & gztacsr (gap-type super-thermal-resistant aluminum alloy steel reinforced) specifications. *J-Power Systems*.

[102] Jim Douglass, Dave; Stewart. Introduction to compact lines. In *EPRI Transmission Line Reference Book — 115-345kV Compact Line Design*. Electric Power Research Institute, 2008.

[103] International Electric Transmission Perception Project, Edison Electric Institute, British Columbia Hydro, United States. Bonneville Power Administration, Electricité de France, Hydro-Québec, and Southern California Edison Company. *Perception of Transmission Lines: Summary of Surveys and Framework for Further Research*. Edison Electric Institute, 1996.

[104] Transmision line reference book: 115-138kv compact line design. 1976.

[105] I. Kishizima, K. Matsumoto, and Y. Watanabe. New facilities for phase-to-phase switching impluse tests and some test results. *Power Apparatus and Systems, IEEE Transactions on*, PAS-103(6):1211 –1216, june 1984.

[106] CIGRE. Guidelines for the evaluation of the dielectric strength of external insulation. *Cigrè Working Group 07 of Cigrè Study Committee 33.*, page Brochure no.72, 1992.

[107] Ian Abi-Samra, Nicholas C.; Grant. Insulation design. In *EPRI AC Transmission Line Reference Book — 200 kV and Above, Third Edition*. Electric Power Research Institute, 2005.

[108] G. Diana, F. Cheli, A. Manenti, P. Nicolini, and F. Tavano. Oscillation of bundle conductors in overhead lines due to turbulent wind. *Power Delivery, IEEE Transactions on*, 5(4):1910 –1922, oct 1990.

[109] K. Tsujimoto, O. Yoshioka, T. Okumura, K. Fujii, K. Simojima, and H. Kubokawa. Investigation of conductor swinging by wind and its application for design of compact transmission line. *Power Engineering Review, IEEE*, PER-2(11):33, nov. 1982.

[110] J. B. Roche and D. A. Douglass. T2 wind motion resistant conductor. *Power Engineering Review, IEEE*, PER-5(10):48 –49, oct. 1985.

[111] Coweta (GA) Wilber F. Powers. Oval shaped overhead conductor and method for making same, 12 1992.

[112] I. Zamora, A.J. Mazon, R. Criado, C. Alonso, and J.R. Saenz. Uprating using high-temperature electrical conductors [overhead power lines]. In *Electricity Distribution, 2001. Part 1: Contributions. CIRED. 16th International Conference and Exhibition on (IEE Conf. Publ No. 482)*, volume 1, page 5 pp. vol.1, 2001.

[113] J.M. Hesterlee, E.T. Sanders, and Jr. Thrash, F.R. Bare overhead transmission and distribution conductor design overview. *Industry Applications, IEEE Transactions on*, 32(3):709 –713, may/jun 1996.

[114] Dave; Goel Anand Wang, Jeff; Havard. Conductor motion. In *EPRI Transmission Line Reference Book — 115-345kV Compact Line Design*. Electric Power Research Institute, 2008.

[115] International Commission on Non-Ionizing Radiation Protection. Icnirp guidelines for limiting exposure to time-varying electric and magnetic fields (1 hz - 100 khz). *Health Physics*, 99(6):818–836, 2010.

[116] The authoritative dictionary of ieee standards terms seventh edition. *IEEE Std 100-2000*, C, 2000.

[117] P. Sarma Maruvada. Corona loss and ozone. In *EPRI AC Transmission Line Reference Book — 200 kV and Above, Third Edition*. Electric Power Research Institute, 2005.

[118] P. Sarma Chartier, Vernon L; Maruvada. Corona and field effects. In *EPRI Transmission Line Reference Book — 115-345kV Compact Line Design*. Electric Power Research Institute, 2008.

[119] F. W. Peek. The law of corona and the dielectric strength of air-iv the mechanism of corona formation and loss. *American Institute of Electrical Engineers, Transactions of the*, XLVI:1009 –1024, jan. 1927.

[120] C. J. Miller. The calculation of radio and corona characteristics of transmission-line conductors. *Power Apparatus and Systems, Part III. Transactions of the American Institute of Electrical Engineers*, 76(3):461 –472, april 1957.

[121] ABB. *ABB Switchgear Manual*. ABB Technical Publications, Zurich, Switzerland, 10th ed. edition, 2001.

[122] U.S. Environmental Protection Agency. Information on levels of environmental noise requisite to protect health and welfare with an adequate margin of safety. *U.S. Government Printing Office*, 1974.

[123] V.L. Chartier and R.D. Stearns. Formulas for predicting audible noise from overhead high voltage ac and dc lines. *Power Apparatus and Systems, IEEE Transactions on*, PAS-100(1):121 –130, jan. 1981.

[124] J.R. Leslie, B.M. Bailey, L.B. Craine, D.C. Eteson, R.E. Grieves, W. Janischewskyj, G.W. Juette, and E.R. Taylor. Radio noise design guide for high-voltage transmission lines. *Power Apparatus and Systems, IEEE Transactions on*, PAS-90(2):833 –842, march 1971.

[125] Vernon L. Olsen, Robert G.; Chartier. Electromagnetic interference. In *EPRI AC Transmission Line Reference Book — 200 kV and Above, Third Edition*. Electric Power Research Institute, 2005.

[126] R. Gutman, P.P. Marchenko, and R.D. Dunlop. Analytical development of loadability characteristics for ehv and uhv transmission lines. *Power Apparatus and Systems, IEEE Transactions on*, PAS-98(2):606 –617, march 1979.

[127] R.N. Nayak, Y.K. Sehgal, and Subir Sen. Ehv transmission line capacity enhancement through increase in surge impedance loading level. In *Power India Conference, 2006 IEEE*, page 4 pp., 0-0 2006.

[128] P.C.V. Esmeraldo, C.P.R. Gabaglia, G.N. Aleksandrov, I.A. Gerasimov, and G.N. Evdokunin. A proposed design for the new furnas 500 kv transmission lines-the high surge impedance loading line. *Power Delivery, IEEE Transactions on*, 14(1):278 –286, jan 1999.

[129] A.R. Bergen and V. Vittal. *Power Systems Analysis*. Prentice Hall, 2000.